EXPERIMENTAL AND DISCRETE ELEMENT SIMULATION STUDIES OF BELL-LESS CHARGING OF BLAST FURNACE

Yaowei Yu

Thermal and Flow Engineering Laboratory
Department of Chemical Engineering
Åbo Akademi University

Åbo, Finland 2013

EXPERIMENTAL AND DISCRETE ELEMENT SIMULATION STUDIES OF BELL-LESS CHARGING OF BLAST FURNACE

Yaowei Yu

Thermal and Flow Engineering Laboratory
Department of Chemical Engineering
Åbo Akademi University

Åbo, Finland 2013

Supervisor

Professor Henrik Saxén

Thermal and Flow Engineering Laboratory

Department of Chemical Engineering

Åbo Akademi University, Åbo, Finland

Opponent and reviewer

Professor Doctor Chuan-yu Wu

Department of Chemical and Process Engineering

University of Surrey, Guildford, United Kingdom

Reviewer

Professor Tatsuro Ariyama

Institute of Multidisciplinary Research for Advanced Materials

Tohoku University, Sendai, Japan

ISBN: 978-952-12-2841-4

Painosalama Oy, Turku, Finland, 2013

Preface

The research effort reported in this thesis was carried out during the years 2009-2012 at the Thermal and Flow Engineering Laboratory at Åbo Akademi University, Finland. The research was done within FIMECC and its ELEMET program and was funded by the Technology Development Centre of Finland (TEKES) and the Finnish metals industry. I gratefully acknowledge the financial support which has enabled me to put full-time work effort on the thesis, and I appreciate the freedom I have been given in my research.

I would like to express my gratitude to my supervisor, Professor Henrik Saxén for all the ideas, inspiration and encouragement he has given me throughout the work. I would also like to thank my colleagues at the Thermal and Flow Engineering Laboratory, Andreas Westerlund, Alfred Kjellman and Tamoghna Mitra, for valuable discussions and help in experiments. The staff in the Thermal and Flow Engineering Laboratory is acknowledged for providing help in daily life. In particular, I would also like to thank Timo Karjalahti from Rautaruukki Steel for excellent cooperation and Professor Seppo Louhenkilpi for his help in life at Aalto University.

Finally, I would like to thank my wife Peng Liu for all the love and support she has given me, and our parent for helping me take my mind off the work and concentrate on the really important things in life.

Åbo on August 26th, 2012

Yaowei Yu

Abstract

This thesis presents an experimental study and numerical study, based on the discrete element method (DEM), of bell-less charging in the blast furnace. The numerical models are based on the microscopic interaction between the particles in the blast furnace charging process. The emphasis is put on model validation, investigating several phenomena in the charging process, and on finding factors that influence the results. The study considers and simulates size segregation in the hopper discharging process, particle flow and behavior on the chute, which is the key equipment in the charging system, using mono-size spherical particles, multi-size spheres and non-spherical particles. The behavior of the particles at the burden surface and pellet percolation into a coke layer is also studied. Small-scale experiments are used to validate the DEM models.

Sammanfattning

Masugnen är den dominerande processen för framställning av råjärn som vidareförädlas till stål i konverterprocessen. Masugnen är en stor högtemperatur-reaktor där beskickningen, bestående av agglomererade järnoxider och koks, matas in i toppen medan förbränningsluft blåses in i ugnens nedre del. Kokset som chargerats brinner i ugnens nedre delar och detta ger upphov till varma reducerande gaser som stiger uppåt och på sin väg genom ugnen värmer, reducerar och smälter järnbäraren. I ugnens övre del, där endast gas och fasta faser förkommer, är den radiella fördelningen av beskickningen av central betydelse, emedan den påverkar gasfördelningen som i sin tur är starkt anknuten till värme- och massöverföring och kemiska reaktioner i ugnens övre del. En lämplig fördelning mellan gasen och den fasta sjunkande fasen leder till en god förvärmning av bädden, en effektiv indirekt reduktion av järnoxiderna samt ett lågt tryckfall och en jämn ugnsgång. Dessa faktorer är alla viktiga förutsättningar för effektiv och ekonomisk masugnsdrift.

Beskickningen består av partikelformiga material, där sinter och pellets (och ibland styckesmalm) används som järnbärare och koks som huvudsakligt reduktionsmedel och energikälla för processen. Inmatningen av de fasta materialet sker idag vanligtvis med en s.k. bell-less top, där en roterande ränna fördelar beskickningen i ringformiga lager på bäddens yta. Avsikten med beskickningsstyrningen är att åstadkomma en materialfördelning som ger en balanserad fördelning i ugnens radiella riktning av förhållandet mellan järnoxid och koks, samt leder till en önskad gasfördelning. Chargeringsprocessen är emellertid komplex och flödet och fördelningen samt sjunkningen av de partikelformiga materialen är svåra att förstå och modellera matematiskt.

Inom geotekniken utvecklade emellertid Cundall och Strack (1979) en matematisk metod, Discrete Element Method eller Distinct Element Method (DEM), som beskriver beteendet hos individuella partiklar i ett större partikelflöde, där varje

partikels lägesmässiga rörelse och rotation beaktas, samt interaktion mellan partiklar och mellan partiklar och gränsytor. Metoden är mycket beräkningsintensiv, men med dagens datorer är det möjligt att beskriva upp till en miljon partiklar trots att beräkningstiden blir lång. Metoden har använts för att beskriva ett otal intressanta fall av partikelflöden som existerar inom industrin.

I doktorsavhandlingen utnyttjades DEM för att undersöka en uppsättning delproblem som berör chargering av masugn. I de flesta fallen verifierades simuleringsmodellerna mot resultat från försök med små anläggningar i laboratorieskala, inklusive en 1:10 skalmodell för masugnens övre del försedd med en chargeringsanordning med en roterande ränna (Kjellman 2009). I arbetets initialskede studerades tömning en ficka eller silo fylld med partikelformigt råmaterial. Detta problem har signifikans för förhållandet vid masugnschargering, där råmaterialet tillfälligt lagras i en ovanom chargeringsanordningen belägen ficka, som tömmes när masugnen är redo att ta emot en ny sättning. Vid utflöde i koniska siloer är det ett välkänt faktum att materialet kan strömma antingen i massaflöde eller i trattflöde, beroende på materialegenskaper och konvinkel. I avhandlingens första artikel undersöktes hur pelletformiga partiklar av olika storlek strömmar ur en silo när de vid påfyllningen lagrats i olika konfigurationer. Experiment i liten skala med tre olika pelletstorlekar utfördes och resultaten jämfördes med DEM-simuleringar. Man fann att den matematiska modellen kunde prediktera fördelningen av partiklarna i utflödet förvånansvärt noggrant. Med hjälp av den matematiska modellen studerades även händelseförlopp och variabler som svårligen kan mätas eller observeras under experiment.

Beteendet hos partiklar som från en silo strömmar ned längs en fast ränna studerades därnäst. Partikelströmmen från rännan samlades upp i ett samplingskärl med olika avdelningar, med hjälp av vilka falltrajektorierna för partiklarna kunde studeras. Först utfördes försök med små stålkulor och massandelen som föll i olika avdelningar av samplingslådan registrerades genom vägning. Man fann att resultat från DEM-simuleringar överensstämde mycket väl med de experimentella resultaten. Därefter studerades genom analys av simuleringsresultaten hur partiklarnas lägesmässiga hastighet och rotationshastighet varierade under strömningen längs rännan och vid det fria fallet efter rännans slut. Det visade sig att hastighetsfördelningen tvärs över rännans tvärsnitt hade formen av ett inverterat V medan rotationshastigheten

uppvisade ett motsatt mönster. Detta innebär att de partiklar som påträffas i de yttre delarna av partikelströmmen i rännan roterar våldsamt, med de som rör sig tillsammans med majoriteten i rännans centrala delar har hög hastighet i rännans riktning men låg rotationshastighet.

Analysen utsträcktes därefter till att omfatta också pelletar och koks. Det visade sig att pelletarna väl kunde beskrivas med en sfärisk partikelmodell, medan man för koks utnyttjade modelleringsmöjligheten att sammanklumpa sfäriska små partiklar till att bilda mer komplexa former. Med dessa modeller kunde relativt väl man beskriva fördelningen av olika massfraktioner av pellet och koks i samplingslådorna. Även den simulerade hastigheten för koks i flödet på rännan verifierades experimentellt. Man fann att beteendet för pelletar och koks avvek sig fundamentalt från varandra och att pelletarna, som är nästan klotformade, uppvisade markant högre rotationshastighet än kokspartiklarna. Även förflyttningshastigheterna var större för pelletarna på rännan, vilket kan förklaras av partiklarnas högre densitet. Generellt befanns utflödeshastigheten från rännan vara högre för de allra första pariklarna i sättningen medan den var lägst för de sista partiklarna som strömmade ut. Under huvuddelen av chargeringsförloppet var dock partiklarnas strömningshastighet i medeltal konstant.

Förhållandena vid chargering och på beskickningsytan studerades även experimentellt och med DEM-simuleringar. T.ex. undersöktes i simuleringarna hur grupper av partiklar beter sig när de strömmar ned på och längs en roterande ränna för att fördelas på beskickningsytan. För att förenkla de experimentella betingelserna chargerades ringar av pellet och koks dels på en horisontell yta och dels på en konformad yta, på vilken kokspartiklar fastlimmats (Sundqvist 2012, Renlund 2012). På detta sätt var starttillståndet för varje experiment identiskt och mätningar av de beskickningsprofiler som uppstod förenklades även. De profiler som uppmättes i experimenten, dels som tvärsnitt observerade genom plexiglas och dels ovanifrån genom analys av bilder från videosekvenser samt med hjälp av en mekanisk mätanordning, användes för att verifiera den matematiska modellen. Man fann att DEM i det stora hela kunde beskriva chargeringsförloppen och den beskickningsyta som uppstod. Inspirerad av överensstämmelsen gjordes en mer detaljerad analys av simuleringsresultaten, där man studerade beteendet hos enstaka partiklar när de träffade ytan efter att ha strömmat från rännan. Det kunde konstateras att partiklar

som härrör sig från de yttre delarna av partikelströmmen på rännan uppvisade den högsta rotationshastigheten och därför också var mest benägna att rulla mot väggen efter att ha träffat beskickningsytan. Genom simulering studerades även bildningen av beskickningslager för koks och pellets, där man observerade ett fundamentalt olikt beteende för dessa två partikeltyper, som beror på skillnader i form, storlek, friktionskoefficient och densitet. Slutligen gjordes ett försök att kvantifiera storlekssegregering av pelletpartiklar.

Avhandlingens sista del fokuserades på studier som ökar förståelsen för hur små (pellet)partiklar i ett lager chargerat på större (koks)partiklar påverkas när lagren rör sig nedåt i masugnen och ugnstvärsnittet växer i schaktet. För detta ändamål konstruerades in modell i liten skala (Westerlund 2010), där beteendet hos några lager av koks och pellets kunde studeras genom ett plexiglas när den ena väggen i anläggningen långsamt flyttades utåt och uppåt medan bottenplattan hölls på samma vertikala nivå men expanderade utåt. På detta sätt efterliknades förloppet som partikellagren utsätts för när beskickningen sjunker i masugnsschaktet, vars diameter ökar. Man fann att de pelletar som befann sig nära gränsytan mot kokslagret gradvis började sjunka in (”perkolera”) i kokslagret, i synnerhet i den expanderande väggens närhet. Ytprofilen uppmättes under bäddens expansion och utvecklingen av gränssnittet mellan materiallagren studerades noggrant genom plexiglaset. En intressant observation som gjordes var att den totala porositeten hos bädden trots pelletinträngningen inte ändrades nämnvärt p.g.a. den samtidiga expansionen av koksbäddstrukturen. Efter att information erhållits från experimenten simulerades förloppet med DEM. Pelletarna beskrevs med en sfärisk partikelmodell medan koksen modellerades med sammanklumpade sfärer som bildade partiklar av olika form och storlek. Man fann igen att DEM lyckades representera beteendet hos materiallagren och inträngningen av pelletpartiklarna i tomrummen mellan koksen. Med simuleringar kunde man dessutom studera hur individuella pelletar långsamt sökte sig genom kokslagret. Försöken och simuleringarna gav intressant information om material-gränssnitt i masugnen, som kan utgöra ett betydande strömningsmotstånd för gasen. Slutligen utfördes en detaljerad simuleringsstudie av systemet ifråga, där känsligheten hos resultaten i avseende på olika parametrar som erfordras för DEM undersöktes. Man fann att vissa parametrar, t.ex. storleksförhållandet mellan koks och pelletar samt form hos kokspartiklarna var av kritisk betydelse, medan andra, såsom

expansionshastigheten hos anläggningen samt friktionen mellan partiklar och vägg var av underordnad betydelse.

Sammanfattningsvis kan konstateras att avhandlingen gett upphov till ny information samt ökad förståelse för masugnens komplexa chargeringssystem och beskickningens beteende i processens översta del. Fastän studien har givit nya insikter krävs dock mer forskning innan masugnens beskickning kan styras optimalt för att bemästra förhållandena i masugnens schakt.

List of Publications

This thesis consists of a summary with the following papers as appendices:

I. Yu YW and Saxén H, (2010). Experimental and DEM study of segregation of ternary size particles in blast furnace top bunker model. Chemical Engineering Science 65, 5237-5250.

II. Yu YW and Saxén H, (2011). Analysis of rapid flow of particles down and from an inclined chute using small scale experiments and discrete element simulation. Ironmaking & Steelmaking 38, 432-441.

III. Yu YW and Saxén H, (2012). Flow of pellet and coke particles in and from a fixed chute. Industrial & Engineering Chemistry Research 51, 7383-7397.

IV. Yu YW and Saxén H. (2013). Behavior of particles on a rotating chute and at formation of burden layers. Submitted manuscript.

V. Yu YW, Westerlund A, Paananen T and Saxén H, (2011). Inter-particle percolation segregation during burden descent in the blast furnace. ISIJ International 51, 1050-1056.

VI. Yu YW and Saxén H, (2012). Effect of DEM parameters on the simulated inter-particle percolation of pellets into coke during burden descent in the blast furnace. ISIJ International 52, 788-796.

Contribution by the Author

The author of the thesis is the main author of all the papers that appear in the appendices. He has written the first draft of the papers and has revised the papers together with his supervisor. All the DEM simulations described in the papers have been performed by the author. He has also planned and carried out a majority of the experiments described in the papers, except the small-scale charging experiments with the conical burden surface referred to in Paper IV, and the pellet percolation experiments of Paper V, which were carried out by Sundqvist and Westerlund, respectively.

Contents

Chapter 1
Introduction

It is not known when the blast furnace was invented, but the process is known to have been commonly used for iron production in the Nordic countries at least since the 14th century. The production of hot metal in blast furnace ranks foremost amongst all the ironmaking processes. This is not only because of the very high production rate but also due to the high degree of heat utilization that can be achieved in the furnace (Biswas 1981).

For long, the blast furnace was considered a black box, as the processes and phenomena in it were difficult to understand. However, by empirical knowledge, the furnace has been controlled and along with better measurements and mathematical modeling, more insight into the internal state has been gained. The blast furnace can basically be operated by experience by four approaches: charging control, thermal control, slag forming control and blast control. The latter (blast control) includes the pressure, temperature and quantity of air. The raw materials primarily determine slag formation, while the thermal state is influenced by the charging and the blast. Charging and blast control are both main methods to adjust gas distribution in blast furnace, but the latter influences the original gas distribution in the hearth and the former decides the gas distribution primarily in the lumpy zone from the throat to the belly. Therefore, understanding the influence of the burden distribution, burden descent and gas distribution is a necessary prerequisite for developing appropriate strategies for controlling the blast furnace operations. Particularly in the daily operation, it is important to attain proper gas flow distribution and ventilation of the furnace in order to keep the condition stable. Furthermore, burden distribution at the blast furnace top is not only the main decisive factor for gas flow distribution, but also one of the most important factors controlling chemical reactions, heat and mass transfer between gas and solid or liquid, and height and shape of the cohesive zone. Therefore appropriate control of the burden distribution is required in the furnace

operation. This is the reason that a large number of studies concerning the influence of burden properties and burden distribution in the blast furnace have been performed in the past, and are continuing at present and in the future (Doinouchi et al. 1962, Kajiwara et al. 1984, Mcgregor et al. 1994, Saxén et al. 2006, Natsui et al. 2009, Ueda et al. 2010).

The focus of this thesis is on the modeling of the blast furnace charging. The models developed have been used to study particle flow in hoppers, on fixed and rotating chute, burden profile formation and inter-particle percolation in coke layer in the bed. The physical phenomena and the properties of the charging are not excessively complicated to understand, but problems arise because of the lack of direct information about burden distribution in operating blast furnaces. Therefore, from a practical point of view, the focus of research work on the blast furnace charging should be focused on the development of new models by which one can study these phenomena and develop new and better charging strategies.

Chapter 2
Blast Furnace Charging System and Discrete Element Method

2.1 Overview of the blast furnace process

The blast furnace is a complex reactor where iron is reduced from iron-bearing oxides with the help of reducing gas at high temperature. The raw material, referred to as the burden, is charged into blast furnace from the top. It mainly consists of enriched iron ore that has been sintered/pelletized to produce a feed of suitable size and strength to ensure smooth flow without (much) degradation, crushed limestone, and coke. The burden is charged batch-wise at the top of the furnace through a bell charger/bell-less charger. As the burden descends in the shaft of the furnace, its temperature rises and a major part of the iron oxides in the ore is reduced by CO and H_2 in the ascending gas. Near the widest part of the furnace, the belly, the iron ore starts softening and finally melts in the *cohesive zone*, forming molten iron and slag. From this zone downwards the only solid material present is coke. Preheated air at a temperature of 1273-1573 K (Helle 2009) is blown into the hearth of the blast furnace through nozzles, called tuyeres. In front of the tuyeres, combustion zones (raceways) are formed where coke is combusted and releases heat, carbon monoxide and hydrogen. The reducing gas ascends through the dropping zone, cohesive zone and lumpy zone and leaves the furnace at the top with some unoxidized carbon monoxide and hydrogen. Figure 1 shows a schematic overview of the blast furnace process.

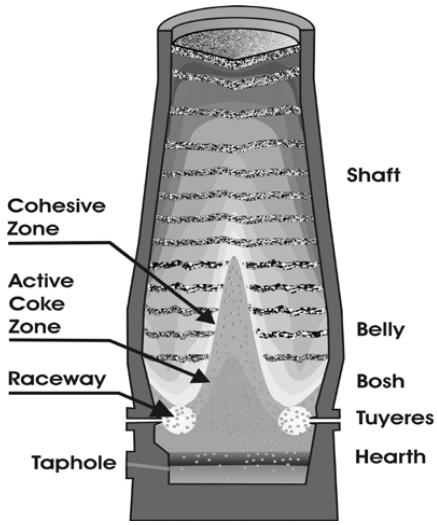

Figure 1. Vertical cross-section of a blast furnace.

2.2 Charging system

Two kinds of charging systems—bell-type and bell-less type—are used in current working blast furnaces. The bell type charging system is still found in small blast furnaces (with effective volumes of 1000 m^3 or less), while bell-less tops appear on intermediate, large, or huge and new blast furnaces, but also in some small ones. The latter charging system has overcome the main disadvantages of the former on the flexibility of charging method and the sealing of large bell, and improved the possibilities for efficient burden distribution control.

Since the first bell-less charging system was invented for the Hamborn company of Germany by E. Legille at Paul Wurth in 1972, there have been two kinds of bell-less charging systems as shown in Fig. 2, namely parallel-type bins and center-type bins. A non-uniformity of the burden distribution across the throat cross-section is a drawback of parallel bins, which was the first type to be invented, because the positions of two material storage bins are not on the center line of the blast furnace. Center-type bins overcome the problem of non-uniform burden distribution, but can be only used under the normal or low smelting intensity rather than high smelting intensity due to the structure of the bins.

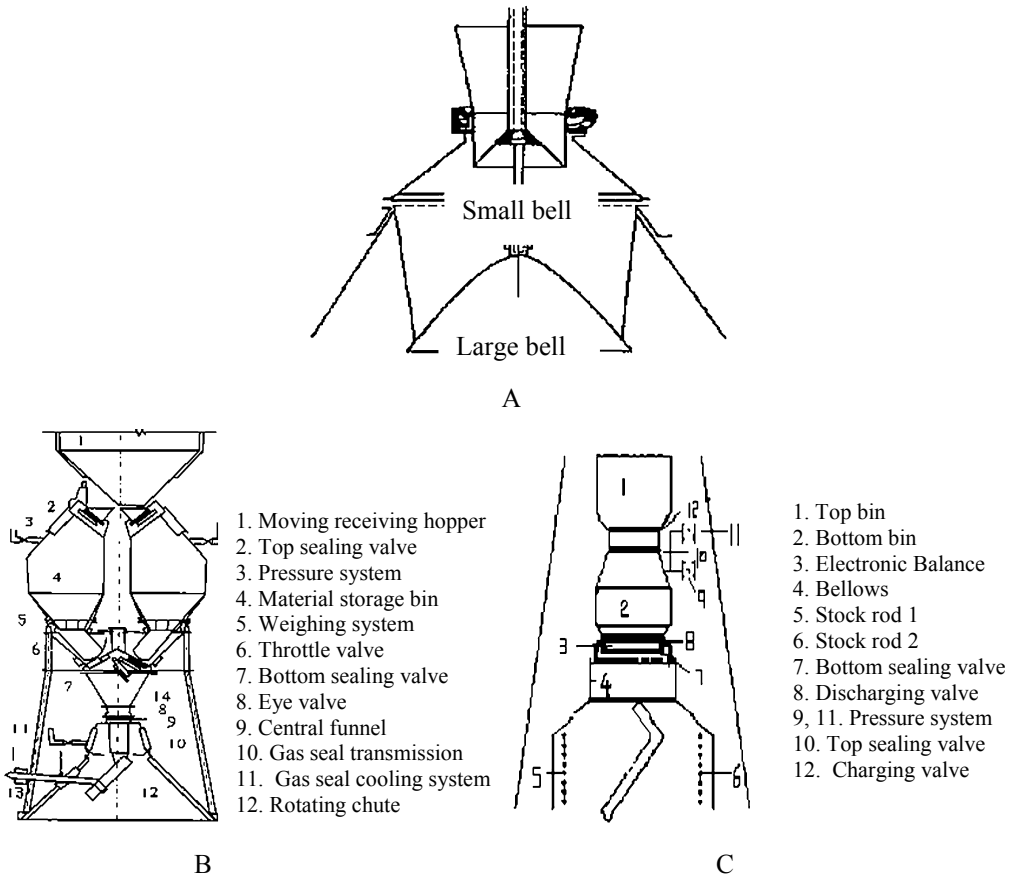

Figure 2. Schematic diagram of equipment structure of bell top and bell-less top (A: bell type B: parallel-type bins, C: center-type bins (Liu 2005, Yu 2008)).

Using the bell-less type charging equipment one can often reach a desired burden distribution flexibly, which indicates that a desired gas distribution can also be obtained. The basic four charging methods are one point charging, multi-ring charging, single ring charging and sector charging (cf. Fig. 3) where one point means the chute doesn't move at all and the sector indicates chute can rotate in a little region. When the inclination angle of the chute is large enough for single ring charging, the burden distribution is quite similar to the "V" shape burden distribution achieved with bell-type charging systems. If the angle of the chute is quite small for a single ring, the distribution resembles the "M" shape burden distribution also found in bell-top furnace. This means that bell-less charging system can mimic the full function of bell-type one, and a flat burden distribution can be realized by multi-ring charging.

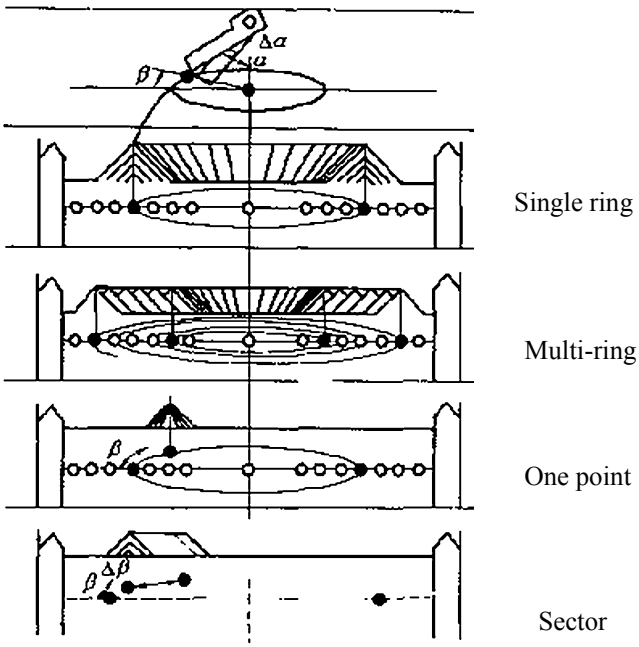

Figure 3. Methods of bell-less distribution (Liu, 2005)

The materials (coke, limestone and iron bearing materials) are transferred into the hopper on the top of the blast furnace by skips (cf. Fig. 4). When the storage bin is empty, the material can enter after the pressure in the storage bin has been reduced to that of the atmosphere by opening the top sealing valve and top throttle valves. After all material has been charged into the bin, the top throttle valve and top sealing valve close. When the stock line has descended to the set-point height, sensed either by mechanical stockrods or by radar, the bottom sealing valve and bottom throttle valve both open, and the material is discharged into the blast furnace through a distributor to the rotating chute, forming new layers on the burden surface. After all material has been charged by the chute, the bottom throttle valve and bottom sealing valve close. The stock rods (or radar) start following the burden surface after the bottom throttle valve closes. After the stock level has reached the set-point, the same charging procedure is repeated for the next material dump.

In this thesis, the material behavior in the blast furnace process from the hopper on the top of the blast furnace to the burden distribution will be investigated.

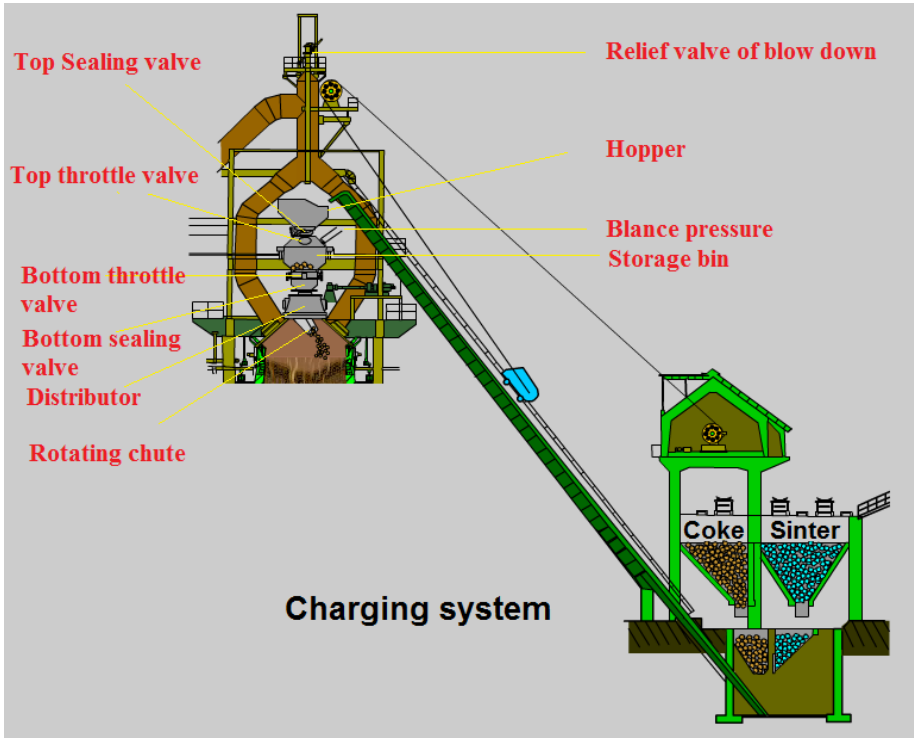

Figure 4. Charging system of blast furnace.

2.3 Discrete element method

From its original development by Cundall and Strack (1979), the discrete element method (DEM) has become a feasible numerical method for analyzing discontinuous media. The technique has already been extensively applied to simulate different granular flows in the industries, including process units such as drum mixers (Kano et al. 2008, Stewart et al. 2001), fluidized beds (Kaneko et al. 1999, Maio et al. 2009), hopper charging and discharging flows (Nguyen et al. 2009, Yu et al. 2010) and flows on inclined chutes (Ho et al. 2009, Mio et al. 2008, 2009, Yu et al. 2011).

The translational and rotational motion of granular particles can be described by Newton's second law of motion combined with a force-displacement correlation at the points of contact between the particles. The DEM used in the current study applies an inter-particle contact model schematically depicted in Fig. 5: A spring and a

dashpot correspond to the elastic and plastic nature of particles in the normal direction, while the model consists of a slider, a spring and a dashpot in the tangential direction. This gives the governing equations for a particle (i) in contact with another particles (j) as (Faug et al. 2003, Zhou et al. 2008, Kurosawa et al. 2012)

$$m_i \frac{d\mathbf{u}_i}{dt} = \sum_{j=1}^{K} (\mathbf{F}_{\mathrm{cn},ij} + \mathbf{F}_{\mathrm{dn},ij} + \mathbf{F}_{\mathrm{ct},ij} + \mathbf{F}_{\mathrm{dt},ij}) + m_i \mathbf{g} \quad (1)$$

$$I_i \frac{\mathrm{d}\boldsymbol{\omega}_i}{\mathrm{d}t} = \sum_{j=1}^{K} (\mathbf{T}_{\mathrm{t},ij} + \mathbf{T}_{\mathrm{r},ij}) \quad (2)$$

where $\mathbf{u}_i$ is the translational and $\boldsymbol{\omega}_i$ the angular velocity, while I_i is the moment of inertia of particle i. The forces acting on the particle are the inter-particle forces and the gravitational force, $m_i\mathbf{g}$. The formers include the normal contact force, $\mathbf{F}_{\mathrm{cn},ij}$, and the tangential contact force, $\mathbf{F}_{\mathrm{ct},ij}$, as well as the corresponding viscous damping forces, $\mathbf{F}_{\mathrm{dn},ij}$ and $\mathbf{F}_{\mathrm{dt},ij}$. The interparticle forces, which depend on the normal and tangential deformations, δ_{n} and δ_{t}, are summed over all the K particles in contact with particle i. The torque acting on particle i includes a component from the tangential force, $\mathbf{T}_{\mathrm{t,ij}}$ and another from the rolling friction, $\mathbf{T}_{\mathrm{r},ij}$. The hardness of the particles and the dashpot are related to Young's modulus and the coefficient of restitution, respectively, while the friction is expressed with a Coulomb-type friction law. The particle forces and torques (see the Appendix) give rise to particle motion, which is integrated from the differential equations (1) and (2), simultaneously considering interaction with other particles and boundaries in the system. Due to the explicit integration method used and the large number of particles in close contact with each other, the time step has to be kept small and the computational effort of the method is considerable. The EDEM software (EDEM 2012) was applied to simulate the motion of the particles in the present study.

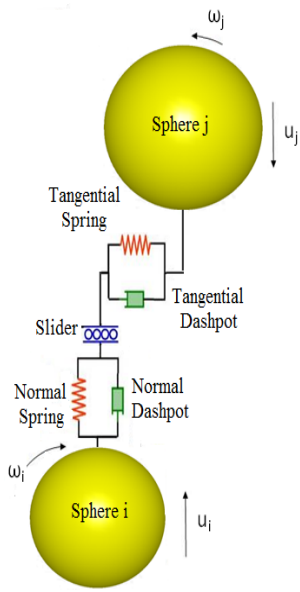

Figure 5. Depiction of interaction forces between two particles in DEM.

Chapter 3
Charging System Modeling in the Literature

In this chapter some modeling and research methods used to investigate blast furnace charging are described and discussed. The focus has been put on research work and methods closely related to or used in the models of this thesis, which are reported in Chapter 4.

3.1 Small or full scale charging model experiments

Small or full scale model experiments (Fig. 6) are performed to study the phenomena and nature of the blast furnace charging process and are also used to validate various mathematical models. The summary of literature in the past was found from the thesis author publication (Yu et al. 2008). The down-scaling from the real size blast furnace to tests in the laboratory is based on the theory of similarity. This is a convenient method to reproduce most phenomena in the charging process, get insight into the principles behind some of the phenomena in charging, and to obtain useful experimental results which can be implemented in the real production environment. However, the costs in terms of money and time required for the setup and experiments are the main drawbacks of physical model tests (Fu et al. 1989, Ichida et al. 1996, Ichida et al. 1991, Kajiwara et al. 1983, Narita et al. 1981, Yamamoto 1958). Another problem is that the results of the experiments may not be general but only of use under some specific conditions (Du et al. 1989, Fu et al. 1989, 1994). Thus, physical model tests are associated with high cost and low flexibility.

Figure 6. Small-scale model equipment: 1:10 blast furnace charging system (Kjellman 2009).

3.2 Artificial intelligence applied to charging

Another approach is to use process data to find the empirical relationships between the parameters, such as top gas analysis and temperature (An et al. 2011) and burden layer thickness (Hinnelä et al. 2003, Pettersson et al. 2003) with data driven methods, such as artificial intelligence. The relationships can be built by artificial neural networks or pattern recognition techniques. Through these relationships, it is possible to throw light on the burden distribution and use the knowledge for optimization of the burden distribution, once a new charging method is proposed. Self-learning functions and online utilization are the primary advantages of the approach, but the relationship deduced only covers the conditions in the furnace that were encountered during the training period, and may therefore not be general. Further, being data-driven, the methods cannot provide fundamental insight into, e.g., why a charging method gives rise to a certain burden distribution.

3.3 Classical mechanics in charging

The bell-less charging system process can be separated into four steps, as shown in Fig. 7: burden movement before the chute, burden movement on the chute, burden movement after the chute (trajectory of burden) and burden distribution in the blast furnace. Knowing the behavior in the previous step, the next step can be calculated: For instance, the end velocity of the particles at the chute tip, can be used as the starting velocity of the burden stream, for which Newton's second law can be applied to solve the trajectory (which in some cases, for the sake of simplicity, is done for one particle only).The impact point of the burden trajectory on the burden surface can then be calculated and a new burden profile can be determined.

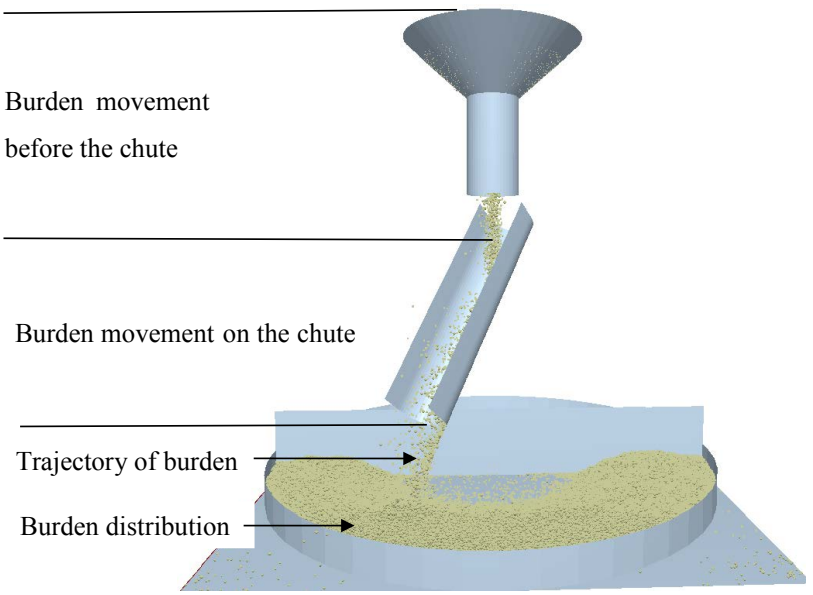

Figure 7. Charging process in a blast furnace.

3.3.1 Burden movement before the chute

Before the burden falls down onto the chute, the material passes through the hopper including the upper hopper and low hopper, or the left hopper and the right hopper,

then falls freely before colliding with the chute. The hopper valve setting determines rate at which material moves out of the hopper. Based on different top equipments of the blast furnace, such as hopper size (Kajiwara et al. 1984, Guan 1995) and hopper valve size (Wang 2003, Gao et al. 2005) or various raw materials, relations between the burden velocity leaving the valve and the opening extent of the hopper wall have been found. However, these relations are specific so the velocity of the materials leaving the hopper valve can only be estimated in blast furnaces with similar equipment. The material velocity before it collides with chute has been calculated by solving the free motion equation from the hopper valve to the chute surface under two different hypotheses: a) Some particles collide with the downcomer pipe in the free fall region (Kajiwara et al. 1984, Ren et al. 1995, Ren et al. 1998, Radhakrishnan et al. 2001, Ren et al. 2003) or b) any particle collision in this region can be ignored (Wang 2003, Liu 2005, Wu et al. 2006).

3.3.2 Burden movement on the chute

As the falling materials collide with the chute, the material velocity after collision will decrease. A common assumption is that the velocity component perpendicular to the chute bottom line can be neglected and the component along the chute bottom line is used as the original velocity of the material entering the chute (Radhakrishnan et al. 2001, Liu 2005, Liang et al. 2009). The material flows through the chute can be modeled by considering moving particle along the chute surface, where the gravitation force ($m\mathbf{g}$), centrifugal force, supporting force of chute (R), friction force of the burden (μR), Coriolis force and burden resistance can be considered, as shown in Fig. 8. Due to the low rotation speed of the chute (typically about 8r min^{-1} in practice) and as the burden resistance only has effect on small size coke (< 10 mm), the Coriolis force and burden resistance have been neglected by most investigators (Liang et al. 2009, Liu 2005, Ren et al. 1998, Radhakrishnan et al. 2001). On the basis of these assumptions, the material velocity leaving the chute tip can be calculated according to Newton's law.

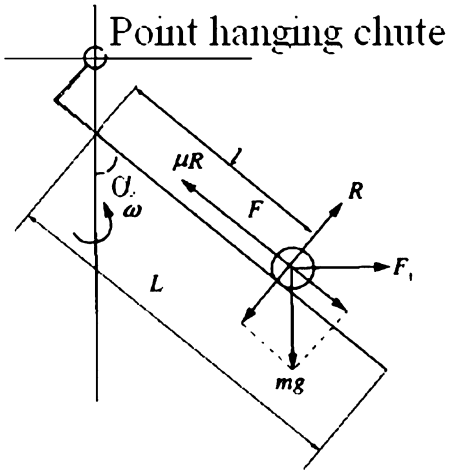

Figure 8. Forces acting on a particle on the chute.

3.3.3 Burden movement after the chute (material trajectory)

The trajectory of materials from the chute tip is important for determining the impact point, where falling materials intersect with the stockline profile which, in turn, determines burden distribution and burden profile. As the stream has a width, three kinds of trajectories can be determined: upper surface flow (Wang 2003), flow of centroid (Kajiwara et al. 1984, Matsuzaki 2003) and lower surface flow (Radhakrishnan et al. 2001), as shown in Fig. 9. After leaving the rotating chute with vertical, radial and tangential components of velocity, the material undergoes free fall till it strikes the stock line. The forces acting on the material are gravitational force, buoyancy force and drag force of gas (Ren et al. 1998). Since the density of the blast furnace gas is small compared to the particle density, the buoyancy forces can be neglected and as the particles used in the charge are fairly large the drag force can also be ignored. Therefore according to Newton's law, the material trajectory (flow of centroid) can be calculated.

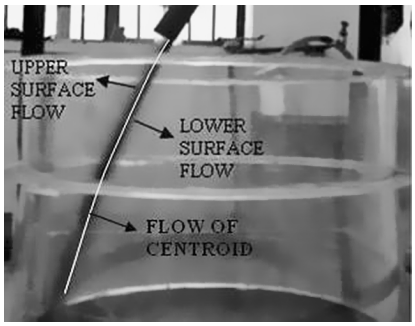

Figure 9. Schematic diagram of trajectories (Yu et al. 2009).

3.3.4 Burden distribution in blast furnace

The burden distribution has two main aspects, namely, burden profile and particle size distribution, because the burden profile determines the ratio of ore to coke (O/C) and particle size distribution influences the porosity of the material layer. Both aspects play an important role for the gas flow distribution in the shaft of the blast furnace. The material, after leaving rotary chute, will fall on the old burden surface and forms a new profile. Burden crest location and repose angles of burden surface (center-side repose angle and wall-side repose angle) are two primary factors determining the new burden profile. The location of the crest (cf. Fig. 10) has often been determined as the intersection point of the centroid of the stream with the old burden surface, except in a few papers (Kajiwara et al. 1984, Okuno et al. 1987).

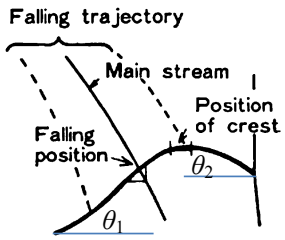

Figure 10. Relation of main stream (flow of centroid) and burden crest (Matsuzaki, 2003).

There is not an agreement about the relationships of repose angles (center-side repose angle (θ_1) and wall-side repose angle (θ_2)), because the burden repose angles are influenced not only by material properties, but also by particle size, moisture content,

stockline height, and gas velocity, as shown in Table 1. However, some consensus is found: Practical repose angles are lower than the natural reposes angles and change with other factors, and even with the charging equipment used. The burden profile can be calculated with the help of the burden repose angles and falling position (cf. Fig. 10), but particle size distribution cannot be investigated any by any classical mechanics method. From the above, it may be concluded that there are several disadvantages of using classical force theory on the charging problem, including the problems of considering the relationship between the hopper valve and velocity of the particles when they leave the hopper, slide along the chute and distribute on the burden surface.

Table 1. Relation between repose angles and other factors. θ_0 is the natural repose angle (°), K a constant (-), H the height of stockline (m) and R the throat radius (m).

Investigators	Expression for θ_1 and θ_2
Liu, Wu et al.*	$\theta_1 = \theta_2,\ tg\theta_1 = tg\theta_0 - K\frac{H}{R}$
Radhakrishman and Ram2001	θ_2 somewhat$<\theta_0$, θ_1 changes with other parameters
Liu 2000	$\theta_1=\theta_0, \theta_2$ from regression equation
Hattori et al. 1993	θ_1 and θ_2 vary with material, chute angle, etc.
Park 1994, Nishio and Ariyama 1990	θ_1 and θ_2 vary with charging equipment & gas velocity

*) Cheng et al. 2006, Gao et al. 2005, Huang et al. 1996, Liu 2005, Wu et al. 2006, 2007, Xu et al. 2005

3.4 Other aspects of burden distribution

3.4.1 Burden descent

As the iron bearing components melt and coke and injectants (pulverized coal, oil, etc.) burn in front of the tuyeres, space will be released and the burden will descend. The burden descent pattern is an important factor which influences the porosity of upper part of the burden, its distribution and the shape of cohesive zone. This is the reason why such a large number of studies concerning the influence of burden descent in the blast furnace have been performed in the past (Ichida et al. 1991a, b, 1996, Kajiwara et al. 1983, Mio et al. 2007, Narita et al. 1981, Saxén et al. 2004).

In almost every blast furnace, there are several (typically two or four) stockrods that sense the burden surface level at several points. An approximate average burden descent rate can be estimated from these measurements, but the information is not sufficient for burden profile calculation. However, the sounding probe information can be used to estimate the burden descent rate distribution. If the descent rate varies linearly with the furnace radius, i.e.,

$$u(r) = a + br \tag{3}$$

where $u(r)$ is the velocity of the burden in the vertical direction at the radial position r, the factors a and b can be derived as

$$a = \frac{r_{\mathrm{rod}} u_{\mathrm{ch}} - \frac{2}{3} R u_{\mathrm{rod}}}{r_{\mathrm{rod}} - \frac{2}{3} R}\ ; \qquad b = \frac{r_{\mathrm{rod}} - u_{\mathrm{ch}}}{r_{\mathrm{rod}} - \frac{2}{3} R} \tag{4}$$

where R is the furnace throat radius and r_{rod} is the distance from the furnace center to the sounding device, u_{ch} is the average velocity of burden descent, given by the volume flow rate of charging material divided by the throat cross-sectional area, and u_{rod} is the burden descent velocity measured by the stockrods.

Figure 11 illustrates the burden descent rate distribution along the radius of blast furnace as measured with a profile meter (Kajiwara et al. 1983). It shows that the burden descent at the wall is faster than in the center which is consistent with findings in the literature (Narita et al. 1981, Mio et al. 2007).

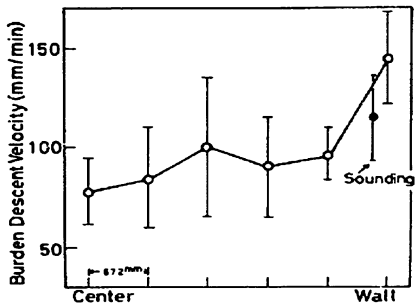

Figure 11. Radial distribution of burden descending velocity (Akiyoshi 1982).

3.4.2 Mixed layer

Sinter and pellets may penetrate into the void between the larger coke particles or push the lighter coke towards the center of blast furnace when they fall on a coke layer, giving rise to a mixed layer (Matsui et al. 2005, Naito 2006) or coke collapse (Austin et al. 2003, Nag et al. 2009). Generally speaking, mixed layers will deteriorate the permeability of burden in the center, but mixed charging of coke and sinter in the center of the blast furnace has also been reported as a new charging practice to reduce the pressure drop and to increase the productivity (Watakabe et al. 2006).

In order to estimate the mixed layer, Kajiwara and co-workers (Kajiwara et al. 1983, 1984) investigated the effect of mixed layer through many experiments, measured it by a magnetometer in several bell-top blast furnaces in Japan and proposed an expression based on the formation energy of the mixed layer (expressed in J), given by

$$E_m = E_k + E_p = \frac{1}{2}mu^2 + mgh \tag{5}$$

where E_k is the collision (kinetic) energy of ore, E_p is the potential energy of ore at the falling point, m is the charged mass of ore in one dump, u is the component of the ore velocity in the direction of the coke surface, and h is the vertical distance between the falling point of the ore and the burden surface at the furnace center. The layer thickness increase of the coke layer, L_c (expressed in m), due to the mixed layer was expressed empirically with the formation energy:

$$L_C = 3.49 \cdot 10^{-4} E_m - 136 \tag{6}$$

The problem with such a semi-empirical equation is that even though it quantifies the thickness of the mixed layer in one point, it does not take a stand on the effect of the coke push on the overall distribution of the burden. Furthermore, the above expression was developed for bell-top charged BFs.

3.5 Discrete element method applied to BF charging

The burden, including coke, sinter and pellets, is composed of granular particles. To predict the behavior of the burden in BF charging, the discrete (distinct) element method (DEM) has become a feasible numerical method, but there are still only a few publications (Ho et al. 2009, Mio et al. 2008, 2009) about DEM applications in the field. Some phenomena, like coke gouge formation that may happen when a heavy material (sinter, pellet or lump ore) falls on a light material (coke) layer, or segregation/sieving/percolation are very hard to simulate using continuum models. DEM is, in turn, well suited to study such phenomena. Using a simplified equipment mimicking a charging device in a blast furnace (Fig. 12), Ho et al., (2009) investigated by three different materials (wood balls, glass balls and steel balls) the impact of charging heavier materials on lighter. Interesting information (the impact on gouge formation) was obtained in the study, but the simplification of the equipment imposes some constraints on the interpretation. Mio et al. (2008 and 2009) studied size segregation of spherical particles charged from a fixed chute and investigated the effect of the chute angle on the charging behavior. Although these studies also yielded interesting findings, a number of important aspects in bell-less blast furnace charging have still not been studied. Therefore, further investigation is needed to gain a deeper understanding of the trajectories and size segregation of the material in the hopper and on the chute, as well as of the arising burden distribution.

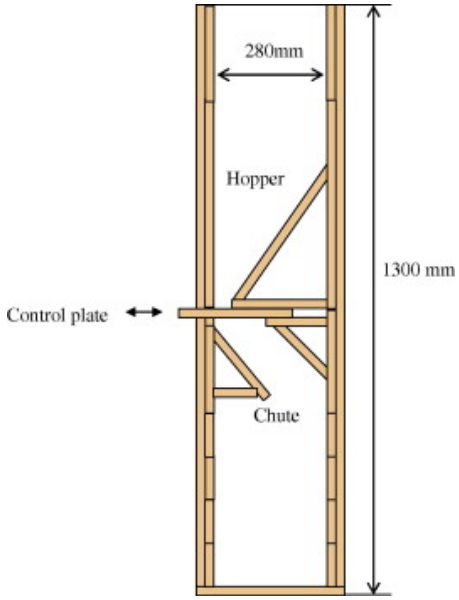

Figure 12. Schematic diagram of the simplified bell-less charging model used by Ho et al. (2009).

3.6 Conclusions of work reported in the literature

The importance of the burden charging on the operation of the blast furnace has been stressed in several publications. Four different recommendations (Section 3.1-3.4) for studying the charging system have been given, but information on size segregation of particles in the hopper and during the hopper discharging process, as well as about the behavior of particles on the chute is still very limited. Furthermore, the layer formation and a possible percolation of smaller particles (e.g., pellets) into a layer of larger particles (e.g., coke) have not been reported in detail. Small or full scale model experiment can reproduce almost all phenomena that occur in the charging process and give information about the features of the charging process, but the costs of setup and experiments are high, the labor involved is considerable and there are small possibilities in practice to rescale the equipment and materials. As for data-driven methods, the access to accurate and sufficient data from the true charging process is a main limitation. Using classical mechanics one can simulate the charging process

from a macroscopic point of view, but considerable simplifications and assumptions have to be made. In practice, the macroscopic phenomena are determined by the microscopic behavior of the particles. Therefore, DEM based on the interactions between the particles is a new feasible numerical method for simulating the blast furnace charging process.

The research work in this thesis concentrates on investigating a new model of the bell-less charging system. Phenomena studied are particle size segregation in the hopper and during the hopper's discharging process, behavior of multi-size spherical particles and non-spherical ones on a chute, burden layer formation in the furnace and pellet percolation in a coke layer during burden descent. The approaches and results are summarized in the following chapter.

Chapter 4
Models Developed in this Thesis

Models for simulation and estimation of the behavior of particles in the blast furnace charging process have been developed in the present work. The models and results of Papers I – VI are briefly presented and discussed in this chapter. The models have been developed and validated using data obtained from experiments with a 1:10 small-scale cold model of the blast furnace charging system (Kjellman 2009) and using other small-scale devices in the laboratory. The investigation was divided into four parts: particle behavior in hopper and during hopper discharging, particle behavior on the chute, burden distribution and burden layer formation, and particle percolation during burden descent.

4.1 Particle size segregation in hopper discharging

In paper I, size segregation during hopper discharge was studied with a small-scale device (Fig. 13). At the beginning of an experiment, mini-pellets of three sizes were charged into the hopper with one of the filling methods (see below), keeping a sliding plate at the exit of the hopper closed. Then, the sliding plate was removed, and the pellets were collected using a 4 ml sample cup and the plate was then quickly closed, repeating this sampling procedure until the hopper was fully discharged. The error introduced by interrupted discharge was also analyzed.

A DEM model with the computational domain and geometry as in the experimental equipment was developed (cf. Fig. 14) and the model was validated by comparison with the experimental results for several different filling methods. After this, a computational study of size segregation during hopper discharging was undertaken.

Figure 13. Photograph of different size pellets and the granular bed in the hopper

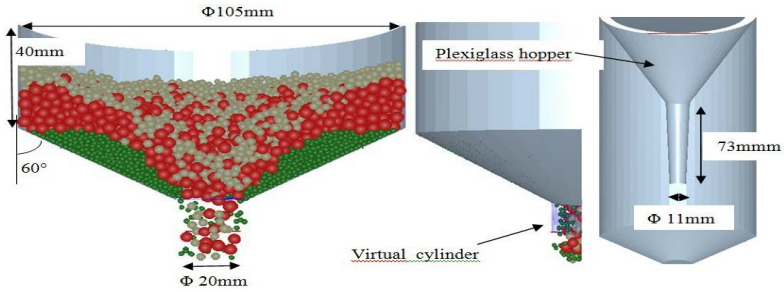

A: Front view B: Left view C: Industrial filling method

Figure 14. Schematic view of (half of) the computational domain of the hopper with coarse particles (red), intermediate particles (gray) and fine particles (dark green)

The hopper was filled by introducing layers of different size pellets in different orders, or by a method named "industrial filling", where a mixture of the particles was gently introduced through a funnel (cf. Fig. 14C). Figure 15 shows a comparison of experimental segregation results (squares, the average of three experiments) with simulation results (circles) with the industrial filling method. The simulation results were found to be in good or excellent agreement with the experimental results, except for some occasional discrepancies that occurred. Therefore, DEM can be considered an appropriate tool for analyzing size segregation during the discharge operation of hoppers filled with (practically) spherical particles.

Size segregation in the hopper discharging process is influenced by many factors, such as the mass fraction of fine materials, the static friction between particles and

wall, and filling method of the hopper. These parameters were investigated numerically in order to provide an improved understanding of the process. The effect of wall-particle static friction on size segregation is illustrated in Fig. 16. Comparing the different curves in the subfigures, the fraction of fine pellets is seen to decrease initially with increase in friction, but increases strongly during the last third of the process, while the coarse particles show an opposite trend. The segregation found is consistent with the observation by Carson et al. (1986). Segregation is aggravated by high static friction especially during the latter half of the process. This explanation can be justified from the distribution of particles at five different discharging stages, plotted in detail in Fig. 17, where the moments are indicated by arrows in the left subfigure of Fig. 16. Fine particles (dark green) collect on the bottom wall surface from point B to point E. This phenomenon is encountered for high wall-particle static friction, clearly seen in subfigure E in the top row of Fig. 17. For the effect of other parameters investigated the reader is referred to Paper I. It should be noted that the effect of particle density, interparticle rolling or static friction and restitution only marginally affect the size segregation in the systems. The extent of segregation was found to be affected mainly by wall-particle rolling and static friction, the fraction of fine particles, the filling method and the diameter ratio of coarse to fine particles. The filling method and the segregation that may occur during this process significantly affect the discharge size segregation. Reducing wall-particle rolling and static friction can reduce the extent of size segregation during the discharging process. If the fine particles in the system represent less than 5% of the total mass the size segregation phenomena are minor.

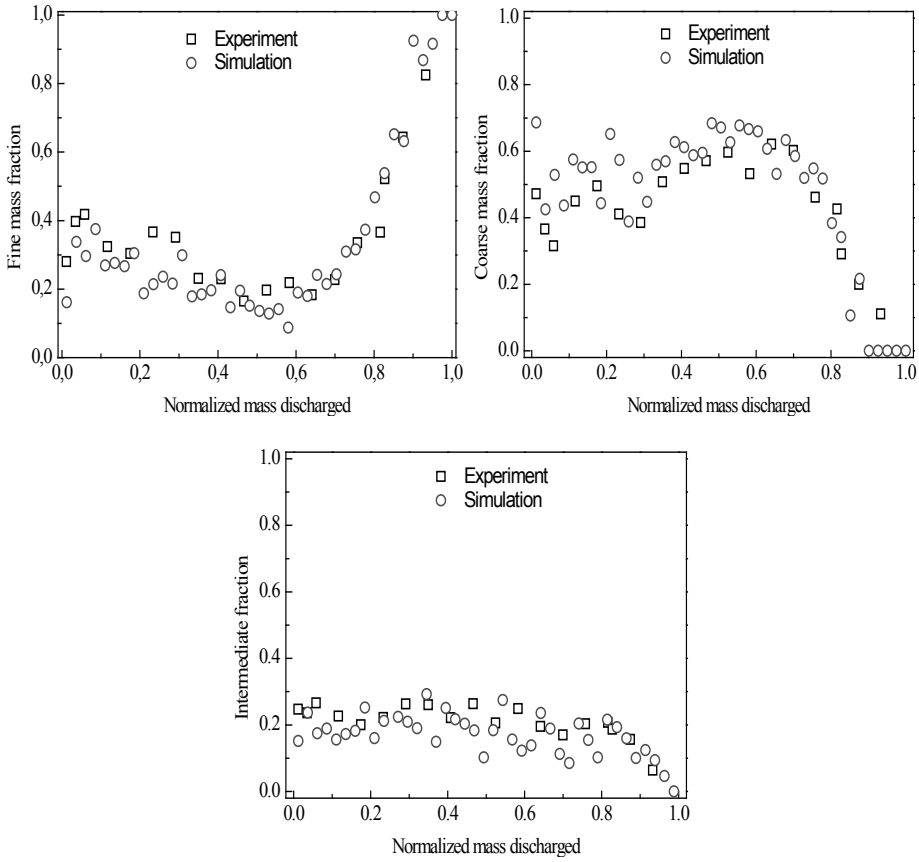

Figure 15. Comparisons of experimental segregation results and simulation results for hopper with industrial filling.

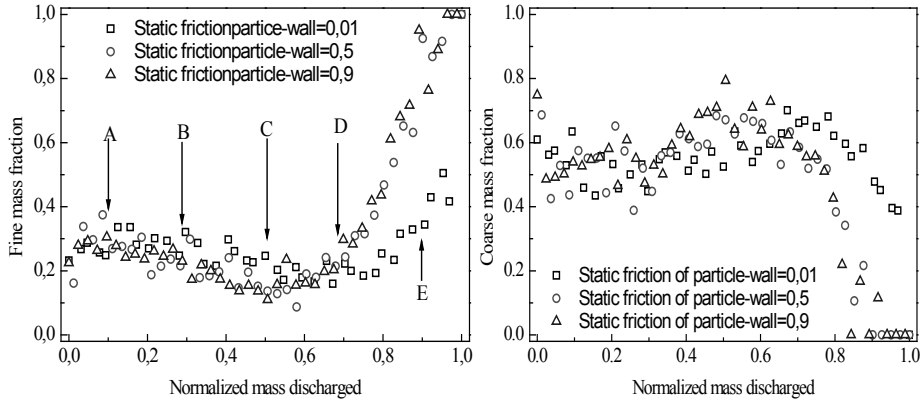

Figure 16. Effects of static friction between wall and particles on size segregation.

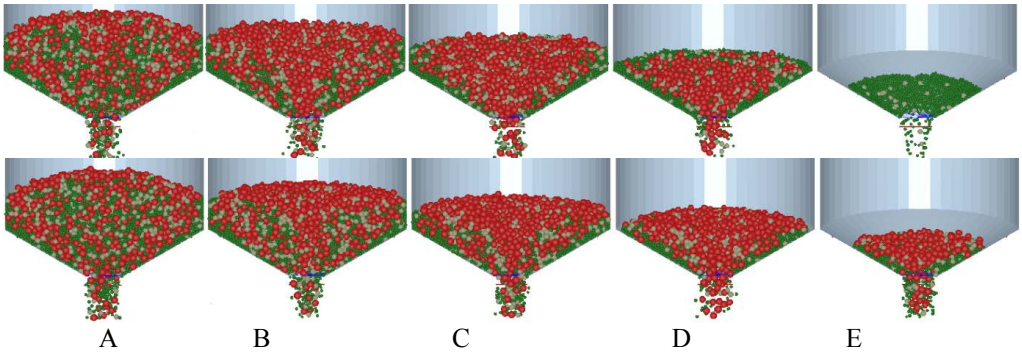

Figure 17. Distribution of different size particles at the five different discharging stages indicated in Fig. 16. Top row: High (0.9) wall-particle static friction coefficient. Bottom row: Low (0.01) particle-wall static friction coefficient.

4.2 Behavior of particles on a fixed chute

The flow of particles on a fixed chute is analyzed in detail in Papers II and III. Three different materials were used to study the phenomena: The basic case studied steel balls, yielding some findings for the behavior of mono-sized spherical particles on the chute. As in Paper I, pellets of three sizes were used to study a multi-size particle system. Finally coke was used to study non-spherical particles. For the sake of simplicity, the chute (scaled by 1:10 in size with respect to the real chute) was fixed and did not revolve in the experiments, but was set in different angles, α (Fig. 18). A multi-box sampling device made of plexi-glass (with 18 compartments) was constructed and placed under the chute tip.

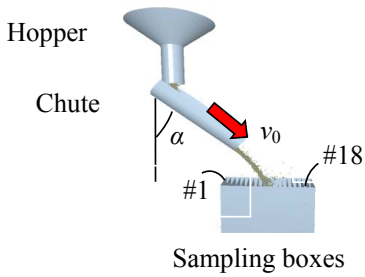

Figure 18. Measuring methods for particle trajectories, velocities and mass fractions in boxes.

A nice agreement is observed in Fig. 19 in a comparison between simulation and experiments of snapshots and mass fractions of trajectories for chutes in different angles, even though some discrepancies are seen to occur for lower values of α. The agreement between the simulation and experiment was not excellent for pellets and coke, but still good and all the main features of the flow of different-sized particles were captured. Figure 20 illustrates the distribution of the simulated angular velocity of the particles along the cross-chute (y) direction at different cross sections, where A, B, C, D denote the locations of the cross sections (cf. Fig. 21) studied in more detail. Every point in the figure represents the average of the angular velocity of the particles encountered within a given interval of y. The angular velocity distribution is clearly V-shaped, with particles with higher rotation at the edges, but the distribution becomes more uniform as the particles flow down along the chute. A lower chute angle is, in general, seen to increase the angular velocities. As for translational particle velocity in the chute, expressed as the square root of the square sum of the three velocity components, the distribution mostly shows an inverted V-shape along the cross-chute direction (Fig. 21). The average translational velocity at the chute tip is practically constant, except at the beginning and the end of discharging process, and it, naturally, depends on the angle of the chute.

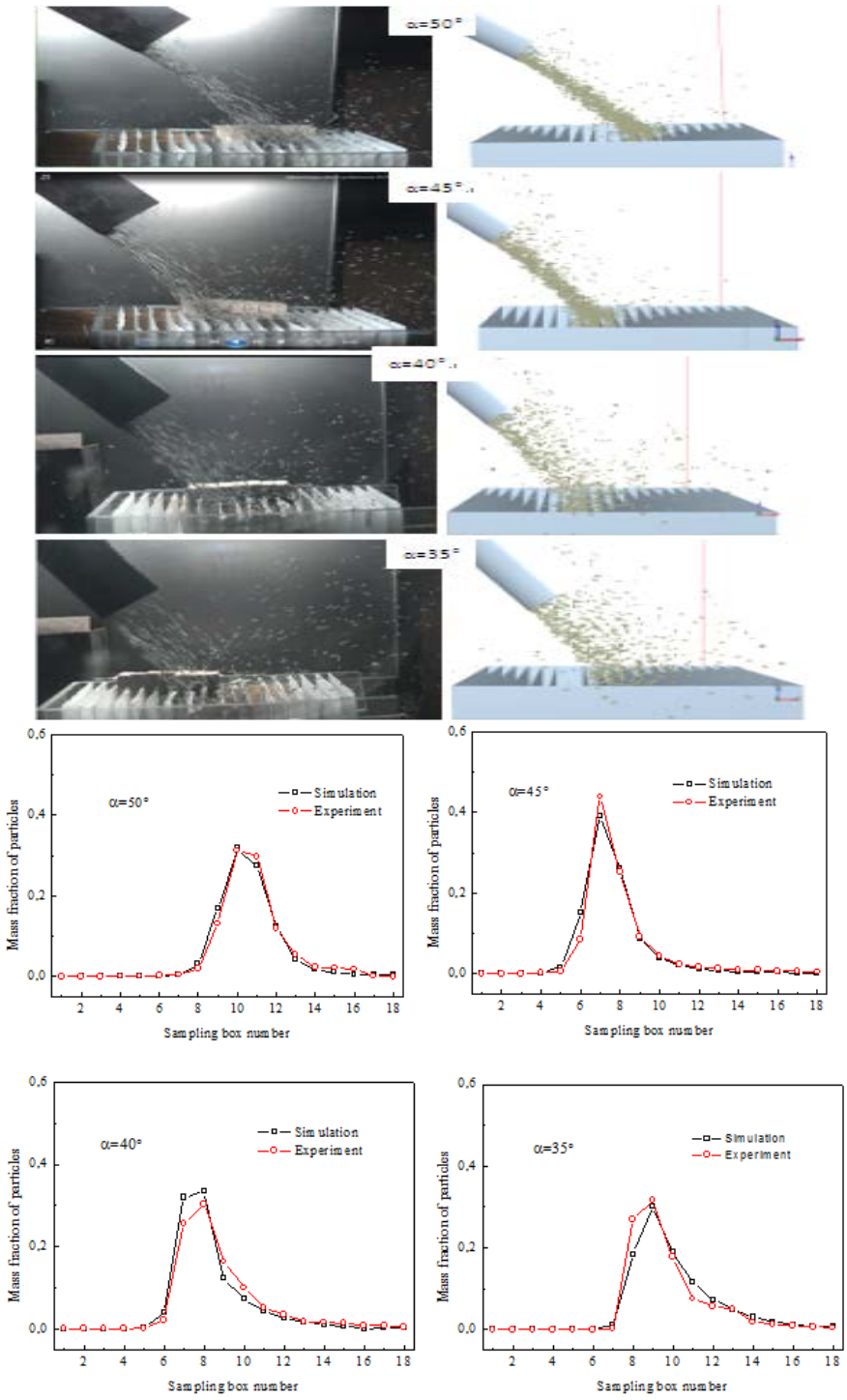

Figure 19. Comparisons of snapshots and mass fractions of steel particle trajectories between experiments and DEM simulation for different chute angles, α.

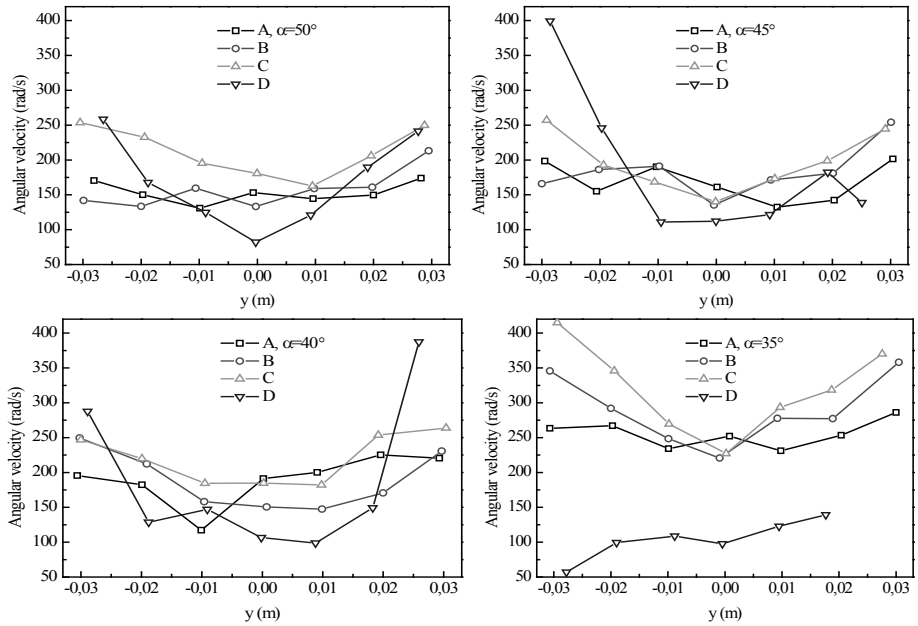

Figure 20. Angular velocity distribution along the *y* direction for different chute angles. Cross sections A-D are indicated in Fig. 21.

Figure 22 illustrates that particles with high velocities at position D collide with the chute and other particles during the hopper discharging process and retard. Both the angular and translational velocities have the feature in common that they become quite uniform as the tip of the chute is approached.

Comparing the behavior of steel balls, pellets and coke, the overall flow patterns are similar. As for the behavior of different size fractions, similar distributions for each size are observed regardless of whether the particles are round (steel balls, pellets) or irregular (coke). The fine particles are primarily found in the inner part of the falling trajectory, whereas larger particles tend to segregate towards the outer parts of the stream. The studies also demonstrated that mono-size particles have a higher mean velocity than multi-size particles in the flow. With the increase of the size distribution of the particles, the mean velocity decreases, because the smaller particles in multi-size particle flow partly occupy the space between the larger particles, which leads to more friction between particles or particles and walls. However, on the angular velocities, the particle shape has a significant influence. When the particle size

distribution widens (from mono- to ternary size), the mean angular velocity increases, mainly because the smaller particles can rotate in the space between larger particles.

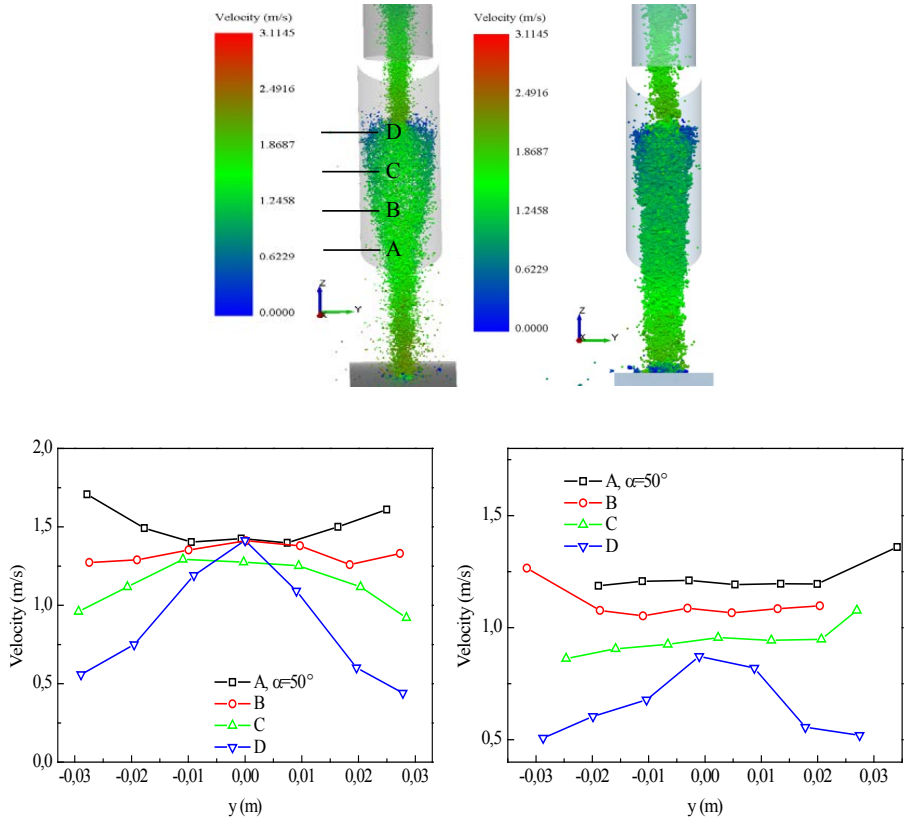

Figure 21. Translational velocity distribution: Pellets (left) and coke (right) in chute (α =50°). The cross sections A-D are indicated in the upper figure.

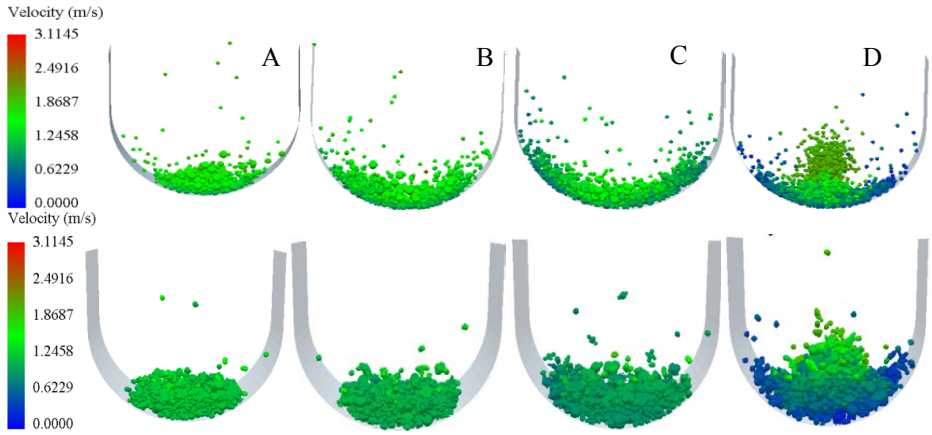

Figure 22. Translational velocity distribution: Pellets (top) and coke (bottom) in chute ($\alpha = 50°$).

4.3 Burden distribution and burden profile

The burden distribution in blast furnaces with bell-less charging systems is formed by a complex pattern of material rings charged at practically arbitrary positions. Therefore, the number of degrees of freedom is almost infinite for longer charging programs, as the size and order of the dumps, number of rings per dump, and chute angles for each dump can be varied. In order to investigate the burden distribution in the work of the present thesis (Paper IV), the study was divided into two parts: burden distribution of different pellet layers and burden distribution including pellet layers and coke layers.

4.3.1 Burden distribution of different pellet layers

In order to investigate experimentally the formation of pellet burden profiles, a laboratory bell-less charging system and a throat of a model blast furnace were used in the experimental work as shown in the top row of Fig. 23. In these experiments, there is a horizontal wooden plate (cf. top right photo, Fig. 23) in the throat which gives a very simple original profile, which is easy to simulate and also reduces the calculating time in the DEM simulation.

Figure 23. Experimental device for bell-less top charging system, with charging on horizontal wooden plate (top right), or in cylindrical throat with a conical base (bottom row).

The pellets used in the experiments consist of ternary size pellets of two different colors (white and black), but only binary sizes of both pellets were used in the DEM simulations, because the mass fraction of the smallest fraction (1-2 mm) is extraordinary low, i.e., less than 5%. Therefore, this mass was included in the 2-2.8 mm fraction in the simulations. In the experiments, the pellet profiles were captured by a high quality camera along two different directions. To reduce the effect of non-uniform flow in the discharging process, different rotation directions (clockwise and anticlockwise) were applied for consecutive rings in both experiments and simulation.

Firstly, white pellets of a given mass were discharged onto the horizontal plate with the chute at α = 43° rotating anti-clockwise, forming the first ring of pellet burden. Secondly, another dump of white pellets of same mass was discharged with clockwise rotation at the same α. Thirdly, the chute angle was decreased to α = 38° while other parameters were kept the same as for the first ring, and finally a fourth ring only changed the chute rotation to clockwise and other parameters were same with the previous. The same procedure was conducted for black pellets. To increase the calculation speed in the simulations of the system, a low shear modulus (10^7 Pa) of

pellets was used, as this yielded no obvious influence on the flow stream or velocities but made it possible to increase the time step in solving the differential equations.

Figures 24 and 25 show comparisons of experimentally observed and simulated pellet profiles. There is only little difference between the left and right burden profiles along the radial direction at the plexi-glass, both in the experiments (1E-8E) and in the simulations (1S-8S) (cf. Fig. 24). Comparing the calculated burden profiles with the experimental one, a quite good consistency is seen, although the pellet pile top at the right profile of the fourth ring (the last white pellet layer) in the experiment is closer to the center than in the simulation, and the left profile of fifth pellet (first black pellet layer) in the experiment is thicker than in the simulation. The top view of Fig. 25 illustrates the same observations. Overall, it can be concluded that the simulations and experiments show good mutual agreement.

Calculated translational velocities of pellets in the chute are shown in Fig. 26. When particles collide with the chute after flowing out from the hopper, they retard considerably and their translational velocity decreases strongly. While the particles flow down the chute their velocity increases steadily to reach a maximum when they leave the chute tip. Due to the friction effect of the chute rotation, pellets no longer move along the bottom center line of the chute but relocate in the direction opposite the rotation direction. This is a macroscopic difference compared to the behavior observed for charging with a fixed chute (cf. Section 4.2).

Burden size segregation along the radial direction is significant in the blast furnace, in particular for particles with a wide distribution, but even for pellets some segregation can be observed. This is next illustrated for the simulated charging of pellet rings. As seen in Fig. 27, there is some segregation for the whole profile including the two pellet types: The larger (black) pellets (mean diameter 3.4 mm) are seen to distribute somewhat more towards the center than the smaller (white) pellets (mean diameter 2.4 mm), but the effect is not remarkable due to the narrow size distribution for both types of pellets (2-4 mm).

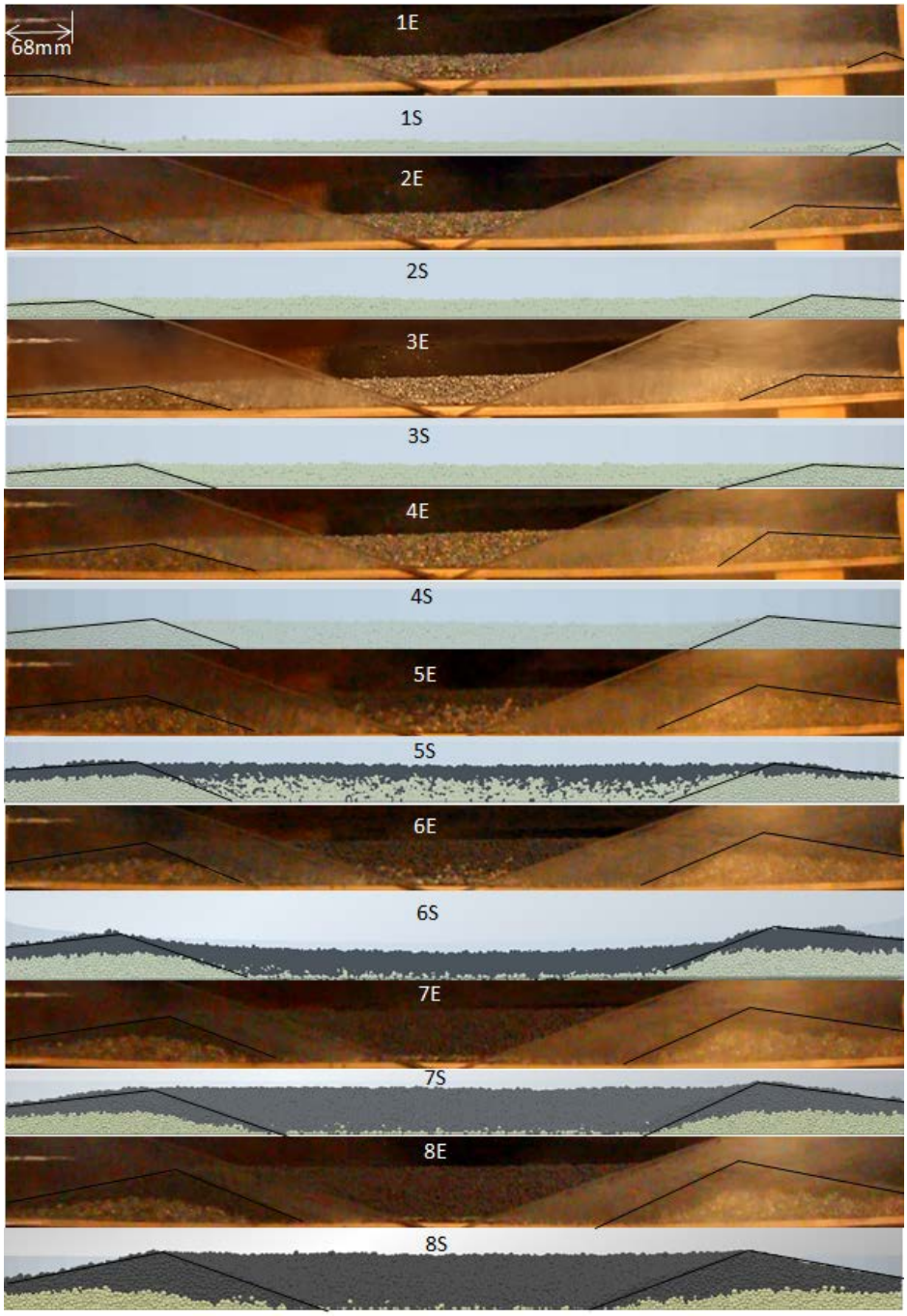

Figure 24. Comparisons of burden distribution along the radial direction in experiment (1E-8E) and simulation (1S-8S) for the eight pellet rings.

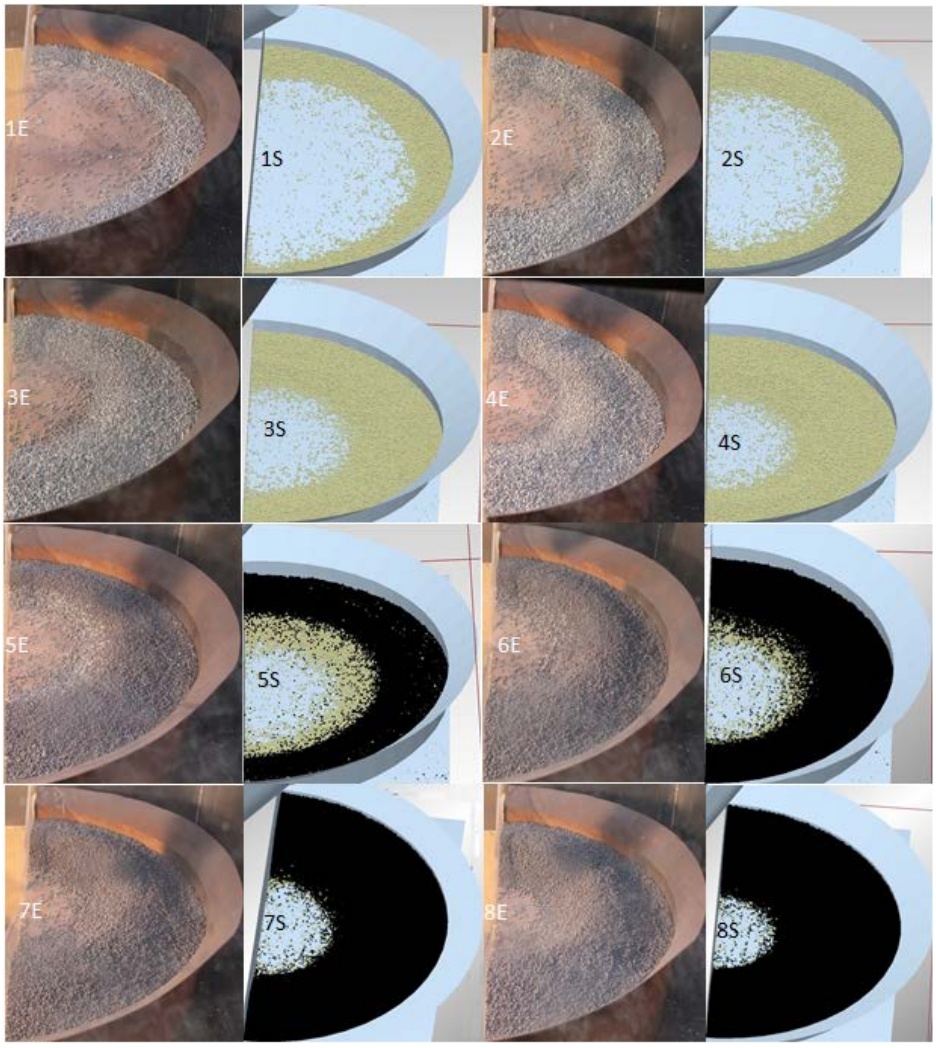

Figure 25. Comparisons of burden distribution at top direction in experiment (1E-8E) and simulation (1S-8S) for the eight pellet rings.

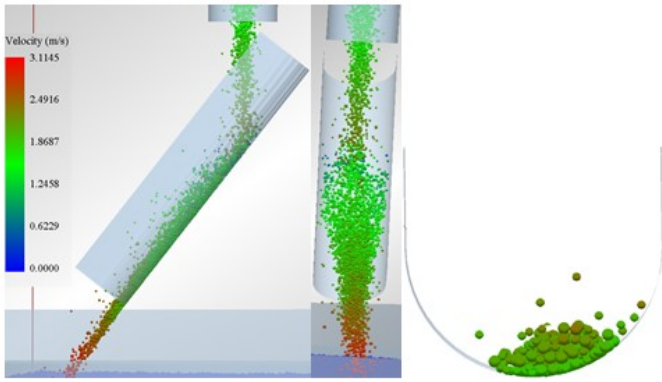

Figure 26. Translational velocity distribution of particles in chute with α=43°.

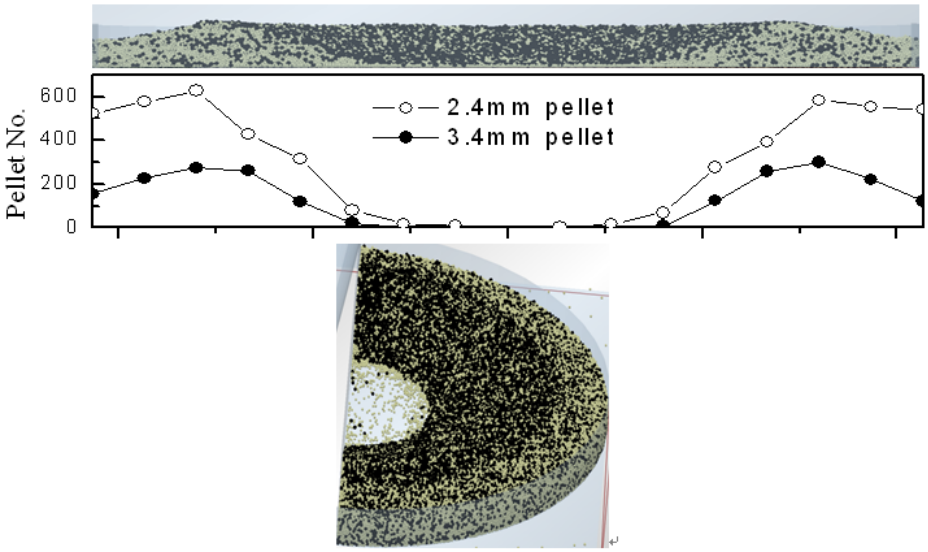

Figure 27. Size segregation in the simulated burden in the radial direction: Situation after the eighth pellet ring.

4.3.2 Burden distribution of coke and pellet layers

In the case to be illustrated next, a steel cone with coke particles glued on top of it was used to represent the initial burden surface (Sundqvist 2012) and vertical steel rods along a diagonal were used to measure the surface profile of each charged layer (cf. Fig. 23). First, a thin layer of pellets was charged on the initial coke profile to

yield the starting point of the experiment (as the last dump to be charged is a big pellet dump). All rings were here charged clockwise and the burden profiles were measured by the steel rods along two diagonals. The first true ring of the sequence, 1.7 kg coke, was charged with chute at α = 31°and chute speed=7.5 r/min. Secondly, another coke dump of same mass was charged with a chute angle of α = 25.5°. This was followed by two pellet rings, 7.45 kg each, charged at angles of α = 43° and 40°, respectively.

Comparisons between the results of the experiments and simulations are provided in Figs. 28 and 29, which show a top view of the bed and the surface profiles after the dumps. In the burden profiles drawn in Fig. 29 the experimental data (markers) represent the average values of four measurement sets along different radial directions. Very few coke particles enter the peripheral region in the experiments, and the same behavior is predicted in the simulation: This is more clearly seen in Fig. 29 than in Fig. 28. The third dump, i.e., the first pellet ring, enters at the wall and covers about one third of the radius, while the second ring of pellets extends the covered region to about half of the radius. Also here the simulation results are consistent with the experimental findings. In summary, a fair or good agreement between burden profiles in experiment and simulation is observed, which demonstrates that the DEM has been able to capture the distribution of the burden particles.

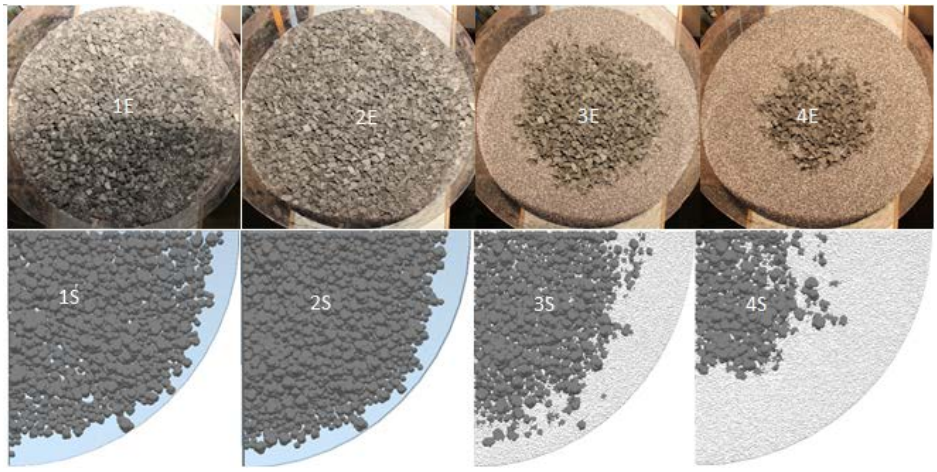

Figure 28. Comparison of top view in experiment (1E-4E) and simulation (1S-4S).

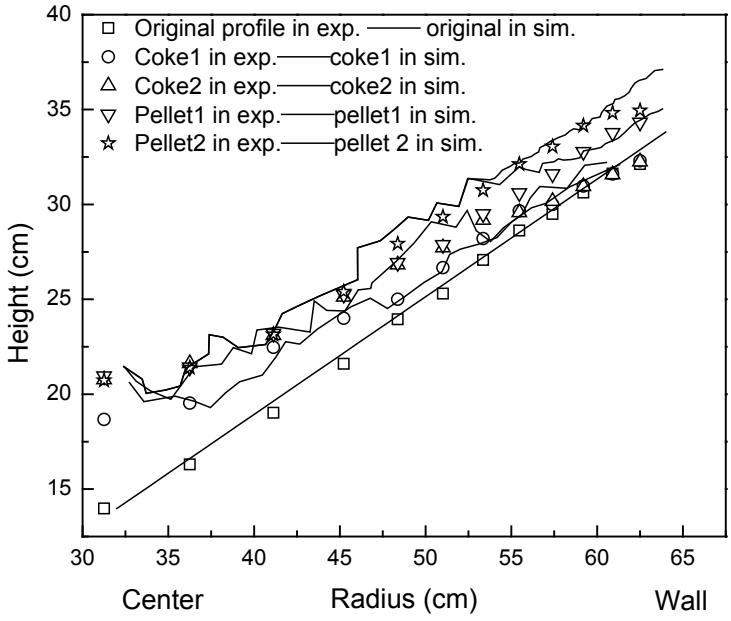

Figure 29. Comparison of burden profile in experiment and simulation.

Figures 30 and 31 show snapshots of the simulated coke and pellet layer formation procedures with the same chute angle α, where each row expresses a whole ring charging at various time instants. It is observed that coke forms piles at the intersection of the flow trajectory with the burden profile. This is so because of a relatively high friction between the particles and as the non-spherical shape of the particles reduces the particle movement. For the pellet rings, however, the particles move to the center, also occupying the space between the larger coke particles after the pellet pile reaches the maximum natural angle.

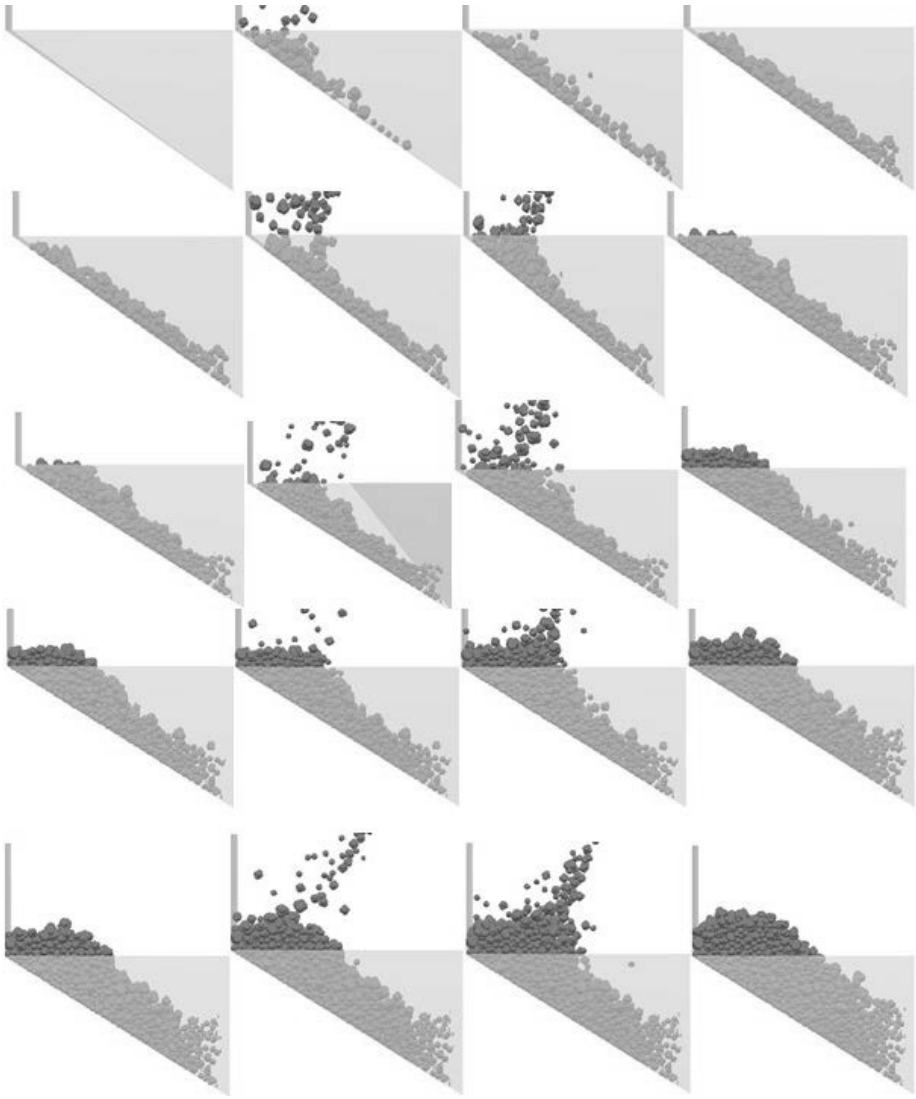

Figure 30. Coke layer formation procedure. Every row represents the formation of one ring on the burden surface at various time instants. Chute angle is the same as in Fig. 31.

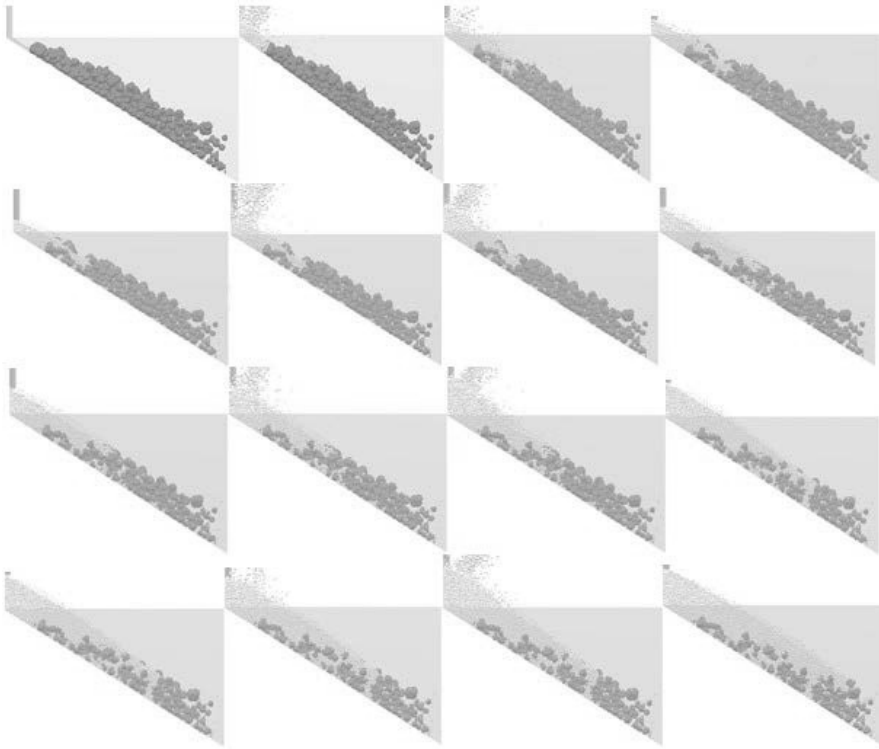

Figure 31. Pellet layer formation procedure. Every row represents the formation of one ring on the burden surface at various time instants. Chute angle is the same as in Fig. 30.

4.4 Pellet percolation in a coke layer

The work in Papers V and VI of the thesis focuses on the inter-particle percolation behavior in the burden during burden descent. A small-scale device simulating the increase in cross-section area associated with the burden descent was constructed (Westerlund 2010), as show in Fig. 32. In the experiments, a layer of coke was first deposited on the bottom of the device, and a layer of pellets was added on its top. After that, the device was slowly (1.5 mm/s in terms of the horizontal motion of the bottom plate) expanded to a maximum expansion of 200 mm, where the left wall (cf. Fig. 32) simultaneously moved left and upwards to mimic the expansion of the cross section of the furnace along with burden descent. The percolation of pellets into the

coke was studied by observations through the plexi-glass and by measuring the heights of the material bed at four positions, with the relative widths of 1/8, 3/8, 5/8 and 7/8 (schematically indicated by triangles in Fig. 32).

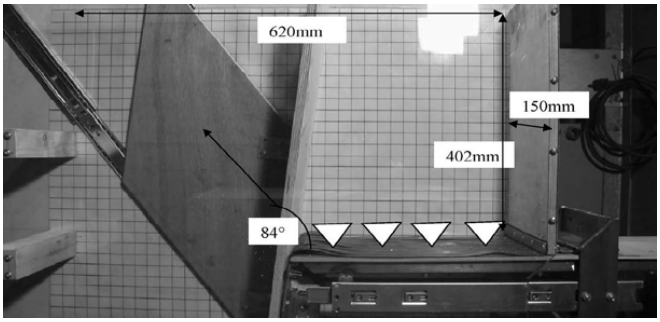

Figure 32. Experimental device for simulation of particle percolation during burden descent.

The procedure of DEM was the same as in the experiment. The left column of Fig. 33 presents results from a percolation experiment with a pellet layer charged upon a coke layer, where the panels correspond to different expansions of the device, starting (at the top) with no (0 mm) and ending (at the bottom) with maximum (200 mm) expansion. The right column of Fig. 33 illustrates the results of a DEM simulation of the particles in the expanding device. The experimental and simulated burden profiles are seen to be in good agreement, and the slight differences can be partly ascribed to the fact that the relatively large coke size distribution is described by particles of three diameters in the DEM and that spherical particles are used in the simulations.

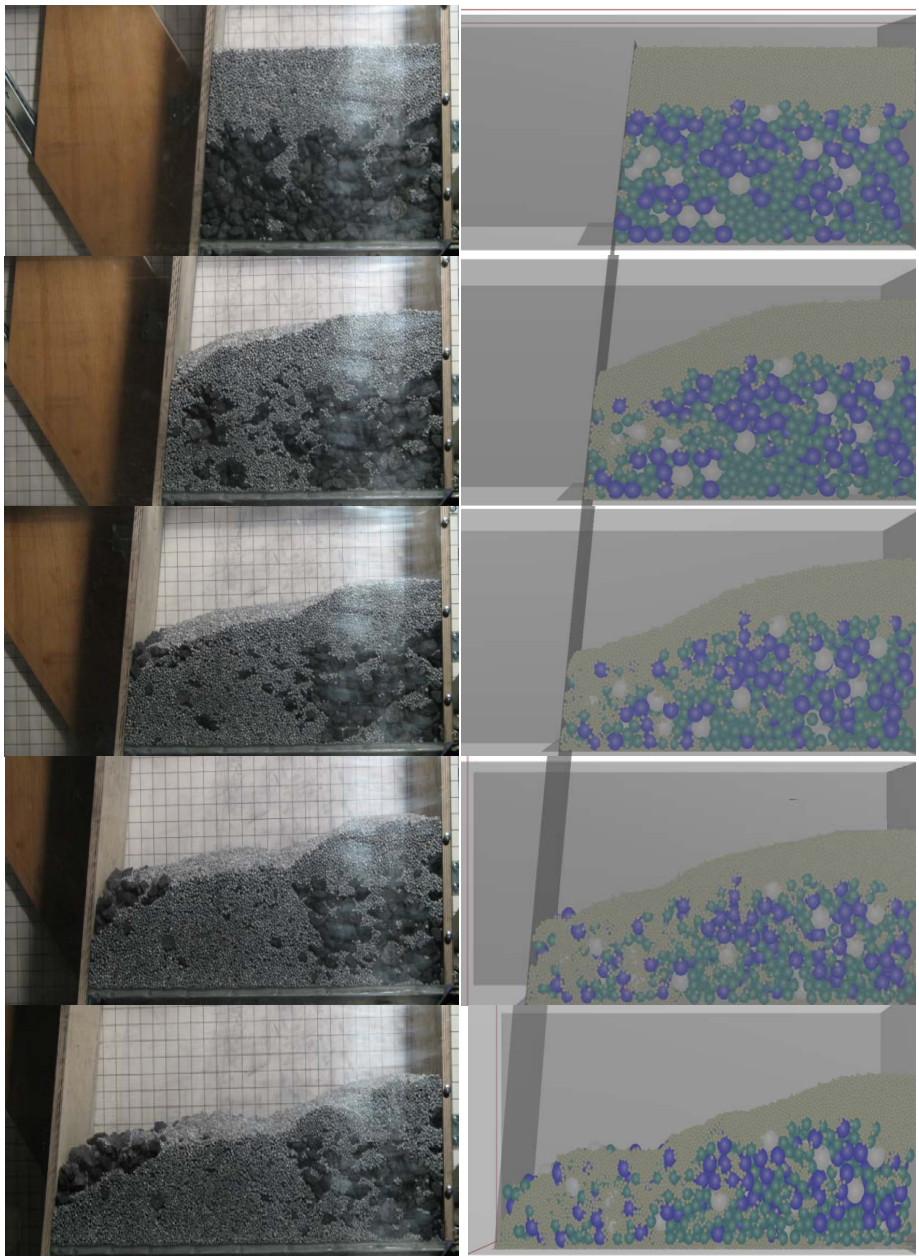

Figure 33. Experimental (left) and DEM simulation (right) results for an expansion experiment with a pellet layer (initial height 62 mm) on a coke layer (initial height 144 mm). Results are illustrated for a device expansion of 0 mm (top) to 200 mm (bottom) with an increment of 50 mm. Coke fractions are illustrated in green (small), blue (intermediate) and white (large), while pellets are depicted in light gray.

In order to illustrate the behavior of the percolating pellet particles, twenty pellets, which eventually percolated throughout the whole coke layer to the bottom plate in the simulation, were selected, with ten from the region close to the moving wall and ten from the center part of the bed (close to the static wall). The traces of these particles are presented in Fig. 34, using dashed-dotted lines for the particles near the moving wall and solid lines for the particles in the center. The percolation behavior is observed to be fundamentally different for the two zones: Close to the moving wall the particle start a rapid descent immediately and five of the particles have reached the bottom plate during the initial 80 mm of expansion, while no pellet particles were found to percolate in the center part of the bed during the first half of the expansion. This serves to illustrate the complexity of the percolation process.

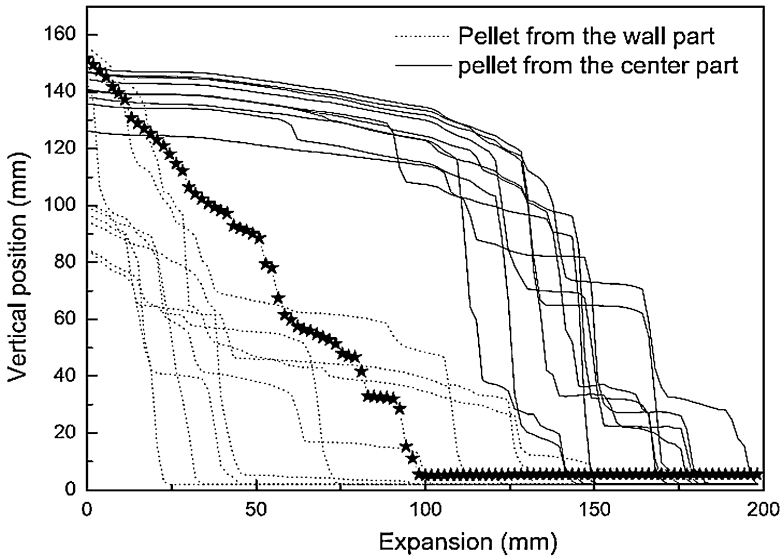

Figure 34. Vertical position as a function of expansion time of twenty randomly selected particles that have descended to the bottom plate at the end of the expansion. Ten particles were selected from the wall part (dashed-dotted lines) and ten from the center part (solid lines) of the bed. The descent of a pellet with a practically constant descent velocity has been indicated by stars.

The results of DEM simulation may strongly depend on the model parameters so it is therefore motivated to carry out a sensitivity analysis of the system studied (Natsui et al. 2010). After the basic study of basic percolation behavior, a parametric study was

undertaken by DEM to analyze the effect of different factors of the extent of percolation, expressed as the mass fraction, *f*, of percolated pellets (Paper VI). The effect of the static friction between the particles and the wall (left inclined moving and right perpendicular wall, as well as wall behind the bed) is illustrated in Fig. 35. With the increase of static friction between pellets and the wall, the mass fraction of percolated particles slightly increases for expansions x>0.5.

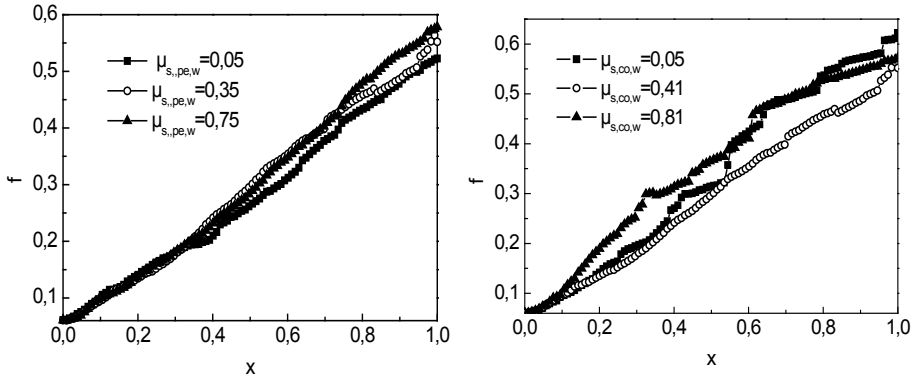

Figure 35. Effect of static friction between particles and wall for pellet-wall (left panel) and coke-wall (right panel) on the mass fraction (*f*) of percolated pellets. The abscissa (x) expresses the dimensionless expansion of the device.

For coke, in turn, the intermediate value of the friction coefficient gives the lowest percolation, while the behavior for a low friction coefficient is irregular. When the friction coefficient is low, the whole coke layer moves as shown in the top panel of Fig. 36, and pellets at the fixed and moving walls percolate strongly into the coke layer. For high value of the static friction between coke and wall (bottom panel), only the coke particles in the lowest part of the layer follow the moving wall, and the pellets roll in this direction and form a surface with a steep inclination. From Fig. 36 it can be concluded that the static friction between the coke and wall mainly controls the layer distribution, but not the extent of percolation. The effect of other parameters on the percolation behavior is explained in more detail in Paper VI.

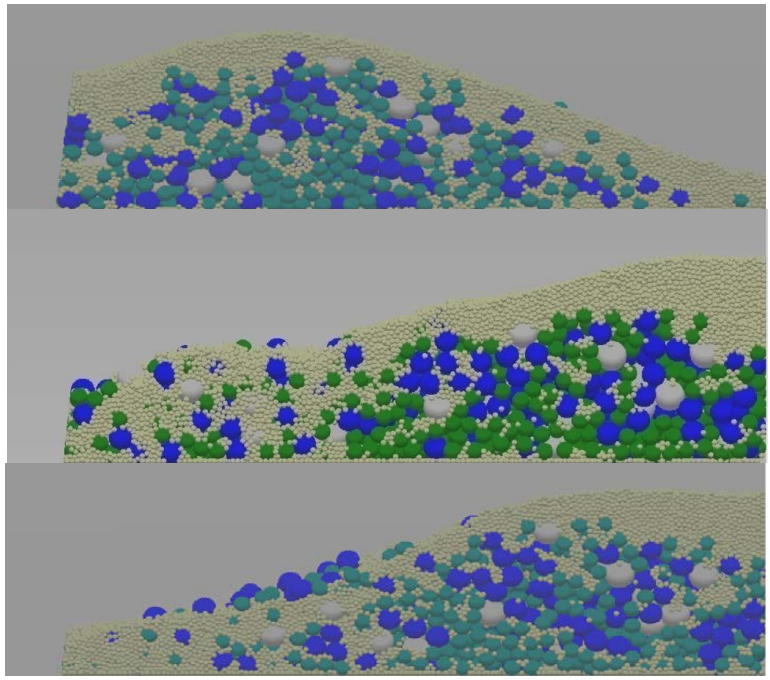

Figure 36. Effect of static friction between coke and the moving bottom plate (top panel $\mu_{s,co,b}$ = 0.05, middle panel $\mu_{s,co,b}$ = 0.41, and bottom panel $\mu_{s,co,b}$ = 0.81) on the percolation behavior at maximum expansion of the device. (Coke1: green, Coke2: blue, Coke3: white, Pellets: light gray.)

4.5 Conclusions

A set of DEM models for simulation and analysis of the burden charging process in the blast furnace has been developed. The main focus has been put on validating the DEM models by comparison with experimental results and investigating some important phenomena in the charging procedure.

Size segregation in hopper discharging, reported in Paper I, was investigated by experiments in small scale and DEM simulation. The results revealed that several important parameters, such as fine mass fraction and the ratio of coarse to fine

particles primarily influence the segregation. However, it must be kept in mind that the results are based on results from an analysis where only one parameter at a time was changed , keeping others at their base values, so the complex interaction between several parameters has not been clarified.

The work reported in Papers II and III studies the behavior of particles flowing on a fixed chute since it is difficult to observe and measure the fast particle flow on a rotating chute. Paper II investigates some properties of the flow of mono-size spherical particles and in Paper III some features of the flow of multi-size spherical and non-spherical particles were studied. As an approximation, the non-spherical coke particles were represented by six non-spherical clumped particles in the simulations. The angular velocity distribution in cross sections of the chute exhibits a V-shaped appearance opposite the distribution of the translational velocity. The fractions of the particles in the trajectories show a similar distribution, regardless of particle size and shape. The mean angular velocity increases and the translational velocity decreases with a growing particle size distribution, while particle shape only influences the angular velocity.

Burden layer formation and distribution were studied in Paper IV and divided into two parts: burden distribution of different pellet layers and burden distribution including pellet layers and coke layers. In order to facilitate DEM simulations with a larger number of particles, reducing shear modulus of the particles in the computation proved to be a feasible method. Studying the formation of pellet rings, only little size segregation was observed. In the cases with coke and pellet charging, coke was found to form piles at the intersection of the flow trajectory with the burden profile, while pellet particles move to the center, partly occupying the space between coke particles on their way after the pellet pile has reached the maximum natural angle. These observations are in agreement with what has been reported in the literature and in practice in other charging experiments.

Particle percolation in the burden layer during descent was studied in Papers V and VI. A new way to observe and study the pellet percolation behavior in a coke layer was proposed and analyzed experimentally and by DEM simulation. The simulations were found to quite accurately reproduce the main results of the experiments, which

illustrates the strength of DEM in throwing light on the complex interaction between particles. However, it must be noted that the results are approximate as the different scaling of the particles and the furnace geometry introduces some bias in the results. Furthermore, the device used in the study cannot mimic the cylindrical geometry of the true blast furnace shaft.

Chapter 5
Future Prospects

The models presented in this thesis have proven successful in extracting new information about the bell-less charging process, burden layer formation and particle percolation during descent in the blast furnace. There are many possibilities to further develop and improve the models, and to use the information gained in future modeling work. Some ideas on how the models can be extended and on new modeling possibilities are discussed here.

The total number of particles including spherical and no-spherical particles in simulation is less than 10^6 which is quite different from the number of real particles (more than 10^9) in the blast furnace charging. Therefore, although the model at present level can describe phenomena in the charging process, there is a long way to go before a realistic number of particles can be considered in the simulations. With the development of software and hardware technology, high speed computers and super computers will resolve this issue in the future. Alternatively, new approaches will be invented to describe flows of a huge number of particles.

Non-spherical coke particles were simply emulated by clumped spherical particles in the work of this thesis, but this is not sufficient for describing the real particles with complex shapes and surfaces. This is, in particular, true for the microscopic properties of coke flow, such as the interaction between coke particles or coke particles and "walls". Therefore, new methods should be found to more accurately simulate the no-spherical particles without excessively increasing the computational burden.

After leaving the chute tip in the charging system, the material flow is influenced by the gas flow in the furnace top, although the influence only has an effect on small size coke (diameters < 10 mm, Ren et al. 1998). The gas flow has also some influence on the burden profile, e.g., the repose angles in the true system. Therefore, considering the gas flow may be significant, and naturally also the arising gas distribution for a

calculated burden distribution. A coupling of DEM with CFD to consider these effects is therefore motivated. The temperature of the blast furnace top gas fluctuates in a wide range (100-500°C) during charging and also varies considerably across the throat. This is, in particular, of practical importance for interpreting above-burden or in-burden probe information appropriately. A coupled CFD-DEM model could consider the effect of such changes in temperature and volume flow rate of the gas, as well as the gas and burden flow lower down in the furnace.

Nomenclature

a	constant
b	constant
e	coefficients of restitution (-)
E	Energy (J), Elastic modulus (Pa)
E^*	Elastic modulus (Pa)
f	mass fraction of percolated pellets (-)
$\mathbf{F}$	force between particles (N)
$\mathbf{g}$	gravity acceleration (m/s^2)
G	shear modulus (Pa)
h	vertical distance between falling point of ore and burden (m)
H	height of stockline (m)
i	general index
j	general index
I	moment of inertia of particle i (kg/m^2)
k	contact coefficient (-)
K	number of particles in contact
L	layer thickness
m	mass of particle (kg)
$\mathbf{n}$	normal vector (from ith to jth particle)
N	number of particles
r	radial coordinate (m)
R	particle or throat radius (m)
t	time (s)
$\mathbf{T}$	torque on particle (Nm)
u	velocity (m/s)
x	coordinate direction (m), dimensionless expansion of device (-)
y	coordinate direction (m)

Greek letters

α	chute angle (°)
δ	deformation (m)
η	damping coefficient (-)
μ	friction coefficient (-)
θ	repose angle (°)
ν	Poisson ratio (-)
ρ	density (kg/m^3)
ω	angular velocity (rad/s)
ω'	angular velocity vector of the object at the contact point(-)

Subscripts

b	bottom plate
c	contact, coke
ch	charging
co	coke
d	deformation
i	*i*th particle
ij	relative quantity from particle *i* to *j*
j	*j*th particle
k	kinentic
m	formation
n	normal
p	potential
pe	pellet
r	rolling
rod	stockrod
s	static
t	tangential
w	wall

Appendix

The expressions for the forces and torques in the DEM model (Eqs. (1-2)) are as follows (Crowe at al., 1998, Renzo and Maio, 2004, Tsuji et al. 1992, Yu and Saxén, 2010, Yu and Saxén, 2011, Zhang et al. 2004):

For the normal contact force we have

$$\mathbf{F}_{\mathrm{cn},ij} = -k_{\mathrm{n}}\delta_{\mathrm{n}}^{3/2}\mathbf{n}; \quad k_{\mathrm{n}} = \frac{4}{3}\sqrt{R_{ij}}E^{*} \tag{A1a,b}$$

where $\delta_{\mathrm{n}} = \left|\boldsymbol{\delta}_{\mathrm{n},ij}\right|$ and the normal vector is calculated as

$$\mathbf{n} = \boldsymbol{\delta}_{\mathrm{n},ij}/\left|\boldsymbol{\delta}_{\mathrm{n},ij}\right| \tag{A2}$$

and the effective radius, R_{ij}, and the equivalent elastic modulus, E^{*}, are given by

$$R_{ij} = \frac{R_i R_j}{R_i + R_j}; \qquad E^{*} = \left[\frac{1-\nu_i^2}{E_i} + \frac{1-\nu_j^2}{E_j}\right]^{-1} \tag{A3a,b}$$

where E and ν are Young's modulus and Poisson's ratio of the particles, respectively.

The normal damping force is written as

$$\mathbf{F}_{\mathrm{dn},ij} = -\eta_{\mathrm{n}}\mathbf{u}_{\mathrm{n,ij}}; \quad \eta_{\mathrm{n}} = 2\sqrt{\frac{5}{6}}\frac{\ln e}{\sqrt{\ln^2 e + \pi^2}}\sqrt{2E^{*}m_{ij}\sqrt{R_{ij}\delta_n}}; \quad m_{ij} = \frac{m_i m_j}{m_i + m_j} \tag{A4a,b,c}$$

where e expresses the coefficient of restitution. The velocities in the normal and tangential directions are

$$\mathbf{u}_{\mathrm{n},ij} = \left(\mathbf{u}_{ij}\cdot\mathbf{n}\right)\cdot\mathbf{n}; \quad \mathbf{u}_{\mathrm{t},ij} = \mathbf{u}_{ij} - \mathbf{u}_{\mathrm{n},ij} \tag{A5a,b}$$

with

$$\mathbf{u}_{ij} = \mathbf{u}_j - \mathbf{u}_i + \boldsymbol{\omega}_j \times R_j\mathbf{n} - \boldsymbol{\omega}_i \times R_i\mathbf{n} \tag{A6}$$

In the tangential direction, the contact force is

$$\mathbf{F}_{\mathrm{ct},ij} = -k_\mathrm{t}\boldsymbol{\delta}_\mathrm{t}; \quad k_\mathrm{t} = 8G_{ij}\sqrt{R_{ij}\delta_\mathrm{n}}; \quad G_{ij} = \frac{G_iG_j}{G_i+G_j} \tag{A7a,b,c}$$

where $\boldsymbol{\delta}_\mathrm{t}$is the tangential overlap and G denotes the shear modulus of the particle, while the damping force is given by

$$\mathbf{F}_{\mathrm{dt},ij} = -\eta_\mathrm{t}\mathbf{u}_{\mathrm{t,ij}}; \quad \eta_\mathrm{t} = 2\sqrt{\frac{5}{6}}\frac{\ln e}{\sqrt{\ln^2 e+\pi^2}}\sqrt{8G_{ij}\sqrt{R_{ij}\delta_n}\, m_{ij}} \tag{A8a,b}$$

under the condition

$$\mathbf{F}_{\mathrm{ct},ij} + \mathbf{F}_{\mathrm{dt},ij} \le \mu_\mathrm{s}\mathbf{F}_{\mathrm{cn},ij} \tag{A9}$$

where μ_s is the static friction. Thus, in Eq. (1) the sum of the two terms in the left-hand side of Eq. (A9) cannot exceed the static contact friction force, $\mu_\mathrm{s}\mathbf{F}_{\mathrm{cn},ij}$.

As for the rolling forces, the torque is given as the vector product

$$\mathbf{T}_{\mathrm{t},ij} = R_i \times (\mathbf{F}_{\mathrm{ct},ij} + \mathbf{F}_{\mathrm{dt},ij}) \tag{A10}$$

while the friction torque is given by

$$\mathbf{T}_{\mathrm{r},ij} = -\mu_\mathrm{r}|\mathbf{F}_{\mathrm{cn},ij}|\boldsymbol{\omega}'; \qquad \boldsymbol{\omega}' = \boldsymbol{\omega}_i/|\boldsymbol{\omega}_i| \tag{A11a,b}$$

whereμ_r is the rolling friction.

References

Akiyoshi K, (1982). Control of Burden Distribution with Profile-Meter for All-Coke Operation of the Blast Furnace, Tetsu to Hagane, 68 (11): 29-29.

An J-Q, Wu M, He Y, Cao W-H, (2011). Soft-Sensing Method of Gas Flow Distribution of Blast Furnace Burden Surface Based on Multi-Level Hierarchical Fusion Algorithm, Acta Automatica Sinica (in Chinese), 37 (4): 496-502.

Austin PR, Chew SJ, Giorgio ND, Zulli P, (2003). Recent Blast Furnace Burden Distribution Studies within BHP Steel. The 3rdInt.Congress on the Science and Technology of Ironmaking, Dusseldorf, Germany. p. 598-604.

Biswas AK, (1981). Principles of Blast Furnace Ironmaking.Cootha Publishing House, Brisbane, Australia.

Carson JW, Royal TA, Goodwill DJ, (1986). Understanding and Eliminating Particle Segregation Problems, Bulk Solids Handling, 6 139-144.

Cheng L, Yu Z, Zhou M, (2006). Development and Application of Blast Furance Burden Distribution Model, Iron and Steel (in Chinese), 41 (11): 13-16.

Crowe C, Sommerfeld M, Tsuji Y, (1998). Multiphase Flows with Droplets and Particles.CRC Press, Boca Raton, Florida.

Cundall PA, Strack ODL, (1979). A Discrete Numerical Model for Granular Assemblies, Geotechnique, 29 (1): 47-65.

Doinouchi T, Yatsuzuka T, Shono S, Komaki S, (1962). On a Distribution of Burden Materials in Blast Furnace Practice, Tetsu to Hagane, 48 (11): 1215-1217.

Du H, Xie G, (1989). Gas Distribution Study on Bell-Less Top Blast Furnace Ironmaking (in Chinese), 8 (5): 48-51.

EDEM (2012). Dem Solutions Limited, www.dem-solutions.com. DEM Solutions Limited.

Faug T, Naaim M, Bertrand D, Lachamp P, Naaim-bouvet F, (2003). Varying Dam Heigh to Shorten the Run-out of Dense Avalanche Flows: Developing a

Scaling Lawfrom Laboratory Experiments, Surveys in Geophysics, 24 555-568.

Fu S, Zhou G, (1989). Study on Burden Distribution in Bell-Less Top Blast Furnace, Iron and Steel (in Chinese), 24 (6): 9-13.

Fu S, Zhou G, (1994). A Study on Application of a Mathematical Model for Burden Profile on Pw Top of Blast Furnace No. 2 in Xiangtan Iron and Steel Company, Journal of Wuhan Iron and Steel University (in Chinese), 17 (1): 1-5.

Gao Z, Dai J, Jiang X, (2005). The Simulation Model of Bell-Less Charging System in Jigang 1750m^3 BF, Ironmaking (in Chinese), 24 (5): 33-35.

Guan X, (1995). Characteristies of Iris Type Flow Control Valve of Bell-Less Top for the Now No. 1 BF at Maanshan Iron and Steel Co., Ironmaking (in Chinese), 14 (3): 37-40.

Hattori M, Iino B, Shimomura A, Tsukiji H, Ariyama T, (1993). Development of Burden Distribution Simulation Model for Bell-Less Top in a Large Blast Furnace and Its Application, ISIJ International, 33 (10): 1070-1077.

Helle M, (2009). Data-Driven Analysis of Blast Furnace Tuyere-Level and Hearth Conditions, Doctoral Dissertation,Åbo Akademi University, Turku, Finland.

Hinnelä J, Saxén H, Pettersson F, (2003). Modeling of the Blast Furnace Burden Distribution by Evolving Neural Networks, Industrial and Engineering Chemistry Research, 42 2314-2323.

Ho CK, Wu SM, Zhu HP, Yu AB, Tsai ST, (2009). Experimental and Numerical Investigations of Gouge Formation Related to Blast Furnace Burden Distribution, Minerals Engineering, 22 986-994.

Huang L, Lu H, Liu J, (1996). Physical Simulation of Baogang #4 Blast Furnace Bell-less Top, Journal of Baotou University of Iron and Steel Technology (in Chinese), 15 (2): 63-67.

Ichida M, Nishihara K, Tamura K, Sugata M, Ono H, (1991a). Influence of Ore/Coke Distribution on Descending and Melting Behavior of Burden in Blast Furnace, ISIJ International, 31 (5): 505-514.

Ichida M, Nishihara K, Tamura K, Sugata M, (1991b). Influence of Inner Wall Profile on Descending and Melting Behavior of Burden in Blast Furnace, ISIJ International, 31 (5): 515-523.

Ichida M, Takao M, Kunitomo K, Matsuzaki S, Deno T, Nishihara K, (1996). Radial Distribution of Burden Descent Velocity near Burden Surface in Blast Furnace, ISIJ International, 36 (5): 493-502.

Kajiwara Y, Jimbo T, Joko T, Aminaga Y-i, Inada T, (1984). Investigation of Bell-Less Charging Base on Full Scale Model Experiments, Transactions ISIJ, 24 799-808.

Kajiwara Y, Jimbo T, Sakai T, (1983). Development of a Simulation Model for Burden Distribution at Blast Furnace Top, Transactions ISIJ, 28 1045-1052.

Kaneko Y, Shiojima T, Horio M, (1999). DEM Simulation of Fluidized Beds for Gas-Phase Olefin Polymerization, Chemical Engineering Science, 54 5809-5821.

Kano J, Kasai E, Saito F, Kawaguch T. (2008).Numerical Simulation Model for Granulation Kinetics of Iron Ores. In: T Ariyama, ed. *Recent progress on mathematical modeling in ironmaking 2008*. Tokyo in Japan: The Iron and steel institute of Japan:8.

Kjellman AA, (2009). Design, Construction and Testing of a Pilot Blast Furnace Bell-Less Top Model, Master Thesis. Åbo Akademi University, Turku, Finland.

Kurosawa H, Matsuhashi S, Natsui S, Kon T, Ueda S, Inoue R, Ariyama T, (2012). DEM-CFD Model Considering Softening Behavior of Ore Particles in Cohesive Zone and Gas Flow Analysis at Low Coke Rate in Blast Furnace, ISIJ International, 52 (6): 1010-1017.

Liang D, Yu YW, Bai CG, Qiu GB, Zhang SF, (2009). Effect of Burden Material Size on Blast Furnace Stockline Profile of Bell-Less Blast Furnace, Ironmaking & Steelmaking, 36 (3): 217-221.

Liu Y, (2005). Charging Rules of Blast Furnace.Metallurgical Industry Press, Beijing.

Maio FPD, Renzo AD, Trevisan D, (2009). Comparison of Heat Transfer Models in DEM-CFD Simulations of Fluidized Beds with an Immersed Probe, Powder Technology, 193 257-265.

Matsui Y, Shibata K, Ono R, (2005). The Principle of Blast Furnace Operational Technology and Centralized Gas Flow by Center Coke Charging, Kobelco Technology Review, 26 12-20.

Matsuzaki S, (2003). Estimation of Stack Profile of Burden at Peripheral Zone of Blast Furnace Top, ISIJ International, 43 (5): 620-629.

Mcgregor BK, Betts JP, Mosley JD, Myklebust KL, (1994). Development and Implementation of a Spread Sheet Based Blast Furnace Burden Model. Ironmaking Conference Proceedings, Chicago: David L. Kanagy (Ed.). p. 6.

Mio H, Komatsuki S, Akashi M, Shimosaka A, Shirakawa Y, Hidaka J, Kadowaki M, Matsuzaki S, Kunitomo K, (2008). Validation of Particle Size Segregation of Sintered Ore During Flowing through Laboratory-Scale Chute by Discrete Element Method, ISIJ International, 48 (12): 1696-1703.

Mio H, Komatsuki S, Akashi M, Shimosaka A, Shirakawa Y, Hidaka J, Kadowaki M, Matsuzaki S, Kunitomo K, (2009). Effect of Chute Angle on Charging Behavior of Sintered Ore Particles at Bell-Less Type Charging System of Blast Furnace by Discrete Element Method, ISIJ International, 49 (4): 479-486.

Mio H, Yamamoto K, Shimosaka A, Shirakawa Y, Hidaka J, (2007). Modeling of Solid Particle Flow in Blast Furnace Considering Actual Operation by Large-Scale Discrete Element Method, ISIJ International, 47 (12): 1745-1752.

Nag S, Basu S, Yu AB, (2009). A Static Approach Towards Coke Collapse Modelling in Blast Furnace,Ironmaking and Steelmaking, 37 (7): 509-514.

Naito M, (2006). Development of Ironmaking Technlogy, Nippon Steel Technical Report, 94 2-15.

Narita K, Inaba S-i, Shimizu M, Yamaguchi A, Kobayashi I, Okimoto K-i, (1981). Burden and Gas Distribution Considering Blast Furnace Aerodynamics, Transactions ISIJ, 21 405-413.

Natsui S, Ueda S, Oikawa M, Fan Z, Kano J, Inoue R, Ariyama T, (2009). Optimization of Physical Parameters of Discrete Element Method for Blast Furnace and Its Application to the Analysis on Solid Motion around Raceway, ISIJ International, 49 1308-1315.

Natsui S, Ueda S, Zhengyun F, Kano J, Inoue R, Ariyama T, (2010). Sensitivity Analysis of Physical Parameters in Discrete Element Method Compared with Blast Furnace Cold Model Experiments, Tetsu to Hagane, 96 1-10.

Nguyen VD, Cogné C, Guessasma M, E. Bellenger, Fortin J, (2009). Discrete Modeling of Granular Flow with Thermal Transfer: Application to the Discharge of Silos, Applied Thermal Engineering, 29 1846-1853.

Nishio H, Ariyama T, (1980). Influence of Gas Flow on Burden Distribution in Blast Furnace, Tetsu to Hagane, 66 (13): 1878-1887.

Okuno Y, Matsuzaki S, Kunitomo K, Isoyama M, Kusano Y, (1987). Development of a Mathematical Model to Estimate Burden Distribution in Bell-Less Typer Charging for Blast Furnace, Tetsu to Hagane, 73 (1): 91-98.

Park NS., (1992). Control of Burden Distribution of No.3 B.F. In Pohang Works. Ironmaking Conference Proceedings, Baltimore Maryland: David L. Kanagy. (Ed.) p. 6.

Pettersson F, Hinnelä J, Saxén H, (2003). Evolutionary Neural Network Modeling of Blast Furnace Burden Distribution, Materials and Manufacturing Processes, 18 (3): 385-399.

Radhakrishnan VR, Ram KM, (2001). Mathematical Model for Predictive Control of the Bell-Less Top Charging System of a Blast Furnace, Journal of Process Control, 11 (11): 565-586.

Ren T, Sheng Y, (1995). The Chute Rules on Bell-Less Blast Furnace Iron and Steel (in Chinese), (5): 5-9.

Ren T, Zhao J, Qiao C, (1998). Effect of Burden Resistance on BF Charging, Iron and Steel (in Chinese), 33 (5): 1-8.

Ren T, Jin X, Jing F, (2003). Effect of Bell-Less Chute Besign Paramenters on Burden Distribution in BF, Iron and Steel (in Chinese), 38 (11): 9-11.

Renzo AD, Maio FPD, (2004). Comparison of Contact-Force Models for the Simulation of Collisions in DEM-Based Granular Flow Codes, Chemical Engineering Science, 59 525-541.

Saxén H, Hinnelä J, (2004). Model for Burden Distribution Tracking in the Blast Furnace, Mineral Processing and Extractive Metallurgy Review, 25 1-27.

Saxén H, Pettersson P, (2006). Genetic Evolution of Novel Charging Programs in the Blast Furnace, Transactions of the Indian Institute of Metals, 59 593-605.

Sundqvist, M, (2012). Experimental and Simulation Study of Blast Furnace Burden Distribution - Case Ruukki. M.Sc. thesis, Åbo Akademi University, Finland.

Stewart RL, Bridgwater J, Zhou YC, Yu AB, (2001). Simulated and Measured Flow of Granules in a Bladed Mixer-a Detailed Comparison, Chemical Engineering Science, 56 (19): 5457-5474.

Tsuji Y, Tanaka T, Ishida T, (1992). Lagrangian Numerical Simulation of Plug Flow of Cohesionless Particle in a Horizontal Pipe, Powder Technology, 71 239-250.

Ueda S, Natsui S, Nogami H, Yagi J-i, Ariyama T, (2010). Recent Progress and Future Perspective on Mathematical Modeling of Blast Furnace, ISIJ International, 50 (7): 914-923.

Wang P, (2003). Measurement and Analysis of Burden Flow Trajectory and Width in Bell-Less Top with Tow Concentric Vertical Hoppers, Iron and Steel (in Chinese), 38 (3): 8-12.

Watakabe S, Takeda K, Nishimura H, Nishimura N, Goto S, Uchida T, Kiguchi M,(2006). Development of High Ratio Coke Mixed Charging Technique to the Blast Furnace.ISIJ International, 46 (4): 513-522.

Westerlund A, (2010). Some phenomena related to pellets charging in the blast furnace. M.Sc. thesis, Åbo Akademi University, Finland.

Wu M, Tian C, Cao W, (2006). Study and Application of Burden Distribution Model for Bell-Less BF, Control Engineering of China (in Chinese), 13 (5): 490-494.

Wu M, Xu Y, Cao W, (2007). Design and Application of Burden Distribution Model in Bell-Less Blast Furnace, Journal of System Simulation (in Chinese), 19 (21): 5051-5056.

Xu Y, Wu M, Cao W, (2005). A Blast Burden Distribution Model Based on Information Fusion and Its Application, Information and Control (in Chinese), 34 (6): 647-653.

Yamamoto M, (1958). Distribution of Blast Furnace Burdens in the Furnace Top Charging Equipment and the Charging Level, Tetsu to Hagane, 44 (9): 954-956.

Yu YW, (2008). Study and Development of the Model for Bell-Less Charging of Blast Furnace, Master Dissertation. Chongqing University, Chongqing.

Yu YW, Bai C, Liang D, (2008). The Technical Methods on the Model of Bell-Less Burden Distribtion of Blast Furance, Metallurgical Collections (in Chinese), 174 (2): 1-5.

Yu YW, Bai CG, Zhang ZR, Wang F, Lv DG, Pan C, (2009). Theoretical Calculation and Validation of Burden Trajectory in Bell-Less Top Blast Furnace, Ironmaking and Steelmaking, 36 (7): 505-508.

Yu YW, Saxén H, (2010). Experimental and DEM Sutdy of Segregation of Ternary Size Particles in Blast Furnace Top Bunker Model, Chemical Engineering Science, 65 5237-5250.

Yu YW, Saxén H, (2011). Analysis of Rapid Flow of Particles in and from an Inclined Chute Using Small-Scale Experiments and Discrete Element Simulation, Ironmaking and Steelmaking, 38 (6): 432-442.

Zhang J, Hu Z, Ge W, Zhang Y, Li T, Li J, (2004). Application of the Discrete Approach to the Simulation of Size Segregation in Granular Chute Flow, Industrial and Engineering Chemistry Research, 43 5521-5528.

Zhou ZY, Zhu HP, Yu AB, Wright B, Zulli P, (2008). Discrete Particle Simulation of Gas–Solid Flow in a Blast Furnace, Computers and Chemical Engineering, 32 1760-1772.

ISBN: 978-952-12-2841-4
Painosalama Oy – Turku, Finland, 2013